Fall 2009

Synthesis and environmental adsorption applications of functionalized zeolites and iron oxide/zeolite composites

Karna Nicole Barquist
University of Iowa

SYNTHESIS AND ENVIRONMENTAL ADSORPTION APPLICATIONS OF FUNCTIONALIZED ZEOLITES AND IRON OXIDE/ZEOLITE COMPOSITES

by

Karna Nicole Barquist

An Abstract

Of a thesis submitted in partial fulfillment of the requirements for the Doctor of Philosophy degree in Chemistry in the Graduate College of The University of Iowa

December 2009

Thesis Supervisor: Professor Sarah Larsen

ABSTRACT

Silicalite-1 crystals and hollow tube zeolite structures were synthesized and functionalized with amine and sulfur containing groups. Nanocrystalline zeolites with a diameter of 30-50 nm and external surface areas around 100 m^2/g were functionalized with 3-aminopropyltriethoxysilane (3-APTES) and 3-mercaptopropyltrimethoxysilane (3-MPTMS). The materials were characterized by ^{29}Si magic angle spinning nuclear magnetic resonance spectroscopy and x-ray diffraction. The adsorption of metal ions from aqueous solutions of K_2HAsO_4 and $Na_2Cr_2O_7$ was measured by inductively coupled plasma-atomic emission spectroscopy. The effects of various conditions such as pH and concentration were studied to optimize adsorption. Adsorption on functionalized mesoporous silica (MS) was conducted for comparison to the functionalized zeolites.

Magnetic zeolite/iron composites were prepared using nanoscale and commercial faujasite zeolites. The composites were functionalized with amine groups to facilitate chromate adsorption under acidic conditions. The materials were characterized using nitrogen adsorption, scanning electron microscopy, thermogravametric analysis, FTIR spectroscopy, and Mössbauer spectroscopy. The adsorption of chromium was evaluated using inductively coupled plasma-optical emission spectroscopy (ICP/OES) to monitor solution chromium quantitatively. The removal of the composites with a magnet was demonstrated. The materials were then evaluated for the adsorption of Cr (VI) using ICP-OES to detect chromium.

Iron containing zeolite composites were prepared using nanoscale faujasite zeolites. The composites were functionalized with amine groups and Fe^{3+} ions to facilitate arsenate(As V) adsorption under a variety of pH conditions[1]. The materials

were characterized using nitrogen adsorption, X-ray diffraction, thermogravametric analysis and FTIR spectroscopy, and Mossbauer spectroscopy. The adsorption of arsenic was evaluated using inductively coupled plasma-optical emission spectroscopy (ICP/OES) to monitor solution concentration quantitatively. The removal of the composites with a magnet was demonstrated. Kinetics and pH dependence of the adsorption were studied. Chromate was removed by both the silicalite-1 crystals and the iron composite. Arsenic was removed by the iron containing composites.

Abstract Approved

_____

Thesis Supervisor

_____

Title and Department

_____

Date

SYNTHESIS AND ENVIRONMENTAL ADSORPTION APPLICATIONS OF FUNCTIONALIZED ZEOLITES AND IRON OXIDE/ZEOLITE COMPOSITES

by

Karna Nicole Barquist

A thesis submitted in partial fulfillment of the requirements for the Doctor of Philosophy degree in Chemistry in the Graduate College of The University of Iowa

December 2009

Thesis Supervisor: Professor Sarah Larsen

Graduate College
The University of Iowa
Iowa City, Iowa

CERTIFICATE OF APPROVAL

PH.D THESIS

This is to certify that the Ph.D. thesis of

Karna Nicole Barquist

has been approved by the Examining Committee for the thesis requirement for the Doctor of Philosophy degree in Chemistry at the December 2009 graduation.

Thesis Committee:

Sarah Larsen, Thesis Supervisor

Darrell Eyman

Johna Leddy

Mark Young

aMichelle Scherer

To Dad Mom and Doug and Ben

ACKNOWLEDGEMENTS

I would like to thank my parents and my entire family for believing in me and supporting me throughout my studies. I would also like to thank in so many ways my advisor Dr. Larsen for all her help and support. This would not have been possible without her. I would also like to thank several people who have helped me out working here-Larsen group members pas and present, Kevin, Jim, Ram, Anamika, Beth, Anton, Melissa, Ashish, and Nick-you guys have always been helpful

I would like to thank Jonas Baltrusaitis and the Central Microscopy Research Facility at The University of Iowa for assistance with XPS spectroscopy (data acquisition and analysis), and Drew Latta, Chris Gorski and Michele Scherer for assistance obtaining and interpreting the Mössbauer spectra and the powder XRD patterns. The ACS PRF and the National Science Foundation for funding.

TABLE OF CONTENTS

LIST OF TABLES

LIST OF FIGURES

CHAPTER 1: INTRODUCTION

1.1 Structural Properties of Zeolites

Zeolites are three dimensional crystalline microporous aluminosilicate materials. The term zeolite comes from the Greek words for boil and stone. Natural zeolites occur in many regions of the world, and over 170 types of synthetic zeolites are known. All zeolites consist of tetrahedral silicon and oxygen atoms coordinated with oxygen-Figure 1.1. The oxygen atoms are at the corner of the tetrahedra, with the other atoms at the center. The overall framework consists of many tetrahedra connected through the oxygen atoms on the vertices. Silicon tetrahedra are electrically neutral, while aluminum tetrahedra have an overall negative charge which must be balanced by another atom. These tetrahedra form channels, which lead to an overall crystalline pore structure. The channels can take different shapes in different zeolites. Two common characteristics of separate types of zeolites are silicon to aluminum ratio and pore size/shape. The general formula for the composition of a zeolite is $M_{x/n}[(AlO_2)_x(SiO_2)_y]mH_2O$. The two types of zeolites mentioned here are zeolite Y and silicalite-1, a purely siliceous form of ZSM-5. Zeolite Y has a faujasite type structure, shown in Figure 1.1, with channels of 0.7 nm leading to supercages of 1.2 nm. The pore shape is symmetrical, and the silicon to aluminum ratio is low, typically around 2 or 3. This aluminum leads to a large cation exchange capacity, but fewer surface silanol groups, whereas ZSM-5 has a different, MFI type structure, with sinusoidal channels intersecting straight pores. ZSM-5 has a MFI type structure, as seen in Figure 1.2, with two different 10-member ring pore types. One set is straight and has an elliptical cross section, while the others are sinusoidal channels

which intersect the straight pores at right angles and have a more circular cross section. The pore diameter for this structure is smaller, .54 nm. The silicon to aluminum ratio is extremely high in this type of zeolite, from 20-∞, with ∞ giving the material commonly called silicalite. There is no aluminum in silicalite material, giving a high density of surface silanol groups-4/nm^2[2] and giving a small cation exchange capacity. No sodium or other cation is needed to make up for aluminum tetrahedral charges in silicalite.

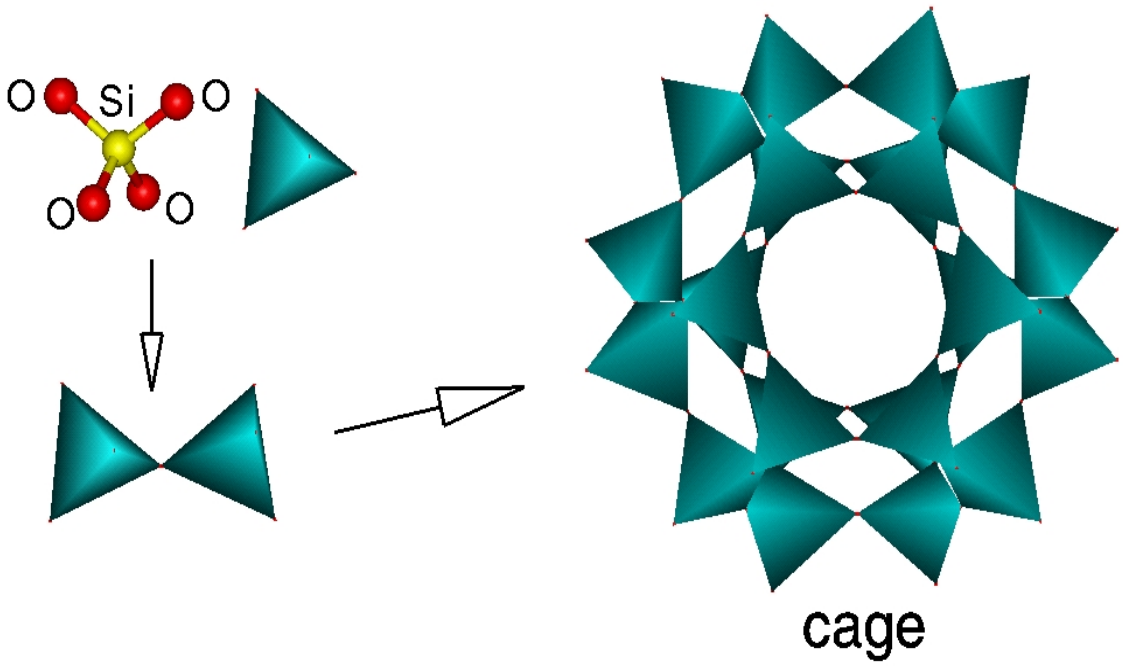

Figure 1.1: SiO_4 tetrahedron, showing the grouping of formations into larger zeolite structures.

Pictorial representations of the frameworks for both MFI type and Faujasite type structures showing their pore shape and structure can be seen on the next page from ref [3]

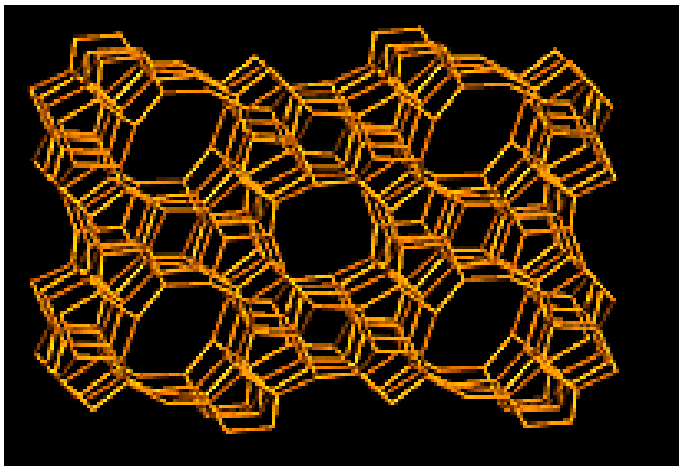

Figure 1.2 MFI framework showing 10-membered ring formation. Silicalite-1 has this framework.

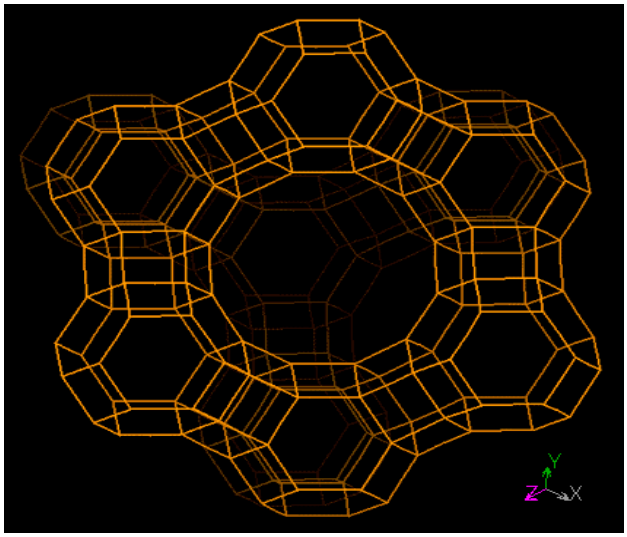

Figure 1.3 Picture of zeolite Y Faujasite type structure.

Zeolites can be synthesized by a variety of methods. Most methods involve a soluble silicon source and a soluble aluminum source reacted under basic conditions,

generally with a quaternary aluminum salt as a structure template[3, 4]. Different pore sizes and different structures can be achieved by using different templates. Recent research has also used coal fly-ash as a material for synthesis[5, 6], and some synthetic techniques have used other crystallizers such as fluoride to crystallize the zeolite material[7, 8].

Zeolite properties can be tuned by changing the silicon to aluminum ratio of the zeolite. Channel structure and particle size also affect the properties of the zeolite. Common properties of zeolites used in commercial applications include ion exchange capacity in powdered laundry detergents and brönsted acidity for petroleum cracking catalysis. The shape and size of pores or channels within the zeolite can make catalysis of one reaction, or diffusion of one product favored over others. Adsorbing molecules of one size or shape over others make zeolites useful in molecular sieving applications.

Nanocrystalline zeolites-usually defined as those with a crystal size of less than 100 nm-are of particular current interest because of the high external surface area. A nanocrystalline zeolite sample with a crystal size of 50 nm has an external surface area of >100 m^2/g or approximately 30% of the total surface area. For comparison, a 500 nm zeolite crystal has less than 10 m^2/g of external surface area, which is less than 3% of the total surface area of the zeolite[3, 4, 9]. The increased external surface of nanocrystalline zeolites provides an additional surface available for adsorption and reaction of molecules. Small crystals have more reactive surface sites than larger crystals. Crystal size is controlled by pH, synthesis ratio, time and temperature. Longer reaction times with lower temperatures lead to smaller crystal sizes. Sodium deficiency in the zeolite synthesis gel is also used to make smaller sizes for the Y type zeolite[10, 11].

Zeolites have a variety of common commercial uses. They are known to be very catalytically active, and are frequently used for adsorption and separations applications. Hydrogen exchanged zeolites are widely used as petroleum catalysts for cracking, isomerisation and fuel synthesis. Ion exchange and ion exchange capacity are also frequently used commercially. "Hard" ions in water, Ca^{2+} and Mg^{2+} are exchanged for Na^{+} ions from the zeolite in the case of the powdered detergents and water softeners. Sodium is specifically related to Si/Al ratio, with each aluminum atom requiring a counter ion. Control of this ratio and therefore the Na^{+} content will allow control of the ion exchange capacity. Other ions can be exchanged either into or out of the zeolites, such as ammonium for soil fertility.

1.2 Functionalization of Zeolites

Functionalization of the surface of a zeolite changes the material in ways determined by the functional group. Properties that can be varied include surface charge, hydrophobicity, molecular binding and reactivity. Adding an organic functional group on the zeolite allows fine tuning of the desired properties. This tuning has become important in applications such as sensing. Methods used for functionalization of silanol groups in silica based materials, such as mesoporous silica[12, 13] can be readily adapted for zeolites with the main difference being that the functionalization occurs exclusively on the external zeolite surface due to the zeolite pore sizes that restrict access to the internal zeolite surface for most organosilane reactants[14]. The advantage of nanocrystalline zeolites in this regard is the extremely high external surface area relative to micron-sized zeolites. Zeolite surfaces can be functionalized by multiple methods- either one pot synthesis, or by post synthesis grafting. Co-condensation, another term

for one pot synthesis, has been applied mainly to mesoporous materials, as they tend to crystallize more easily. This direct method can lead to higher amounts of functionalization, and more even deposition of functional groups, also allowing access to the interior surfaces of the materials[15]. However, co-condensation methods tend to interfere with crystallization, which is problematic in zeolite synthesis. Post synthesis grafting avoids crystallization problems, since the zeolite structure is already formed before any functionalization takes place. Postsynthesis grafting is done using techniques such as silane functionalization, where surface silanol groups are reacted with silanes, as seen in Figure 1.3. These silanes are usually too big to penetrate the zeolite pores, so only external functionalization is possible.

Two different types of functionalization studied are sulfur (thiol/sulfonic acid) and amine. Amine functionalization can be obtained by functionalizing with an aminosilane, such as 3-aminopropyltriethoxysilane (APTES), 2-amine-3-aminotrimethoxysilane, or 3-aminopropyltrimethoxysilane. These will give amine or diamine functionalization. The silane functionalization needs a catalytic amount of water to proceed, but large amounts of water in the silane or the solvent can lead to deactivation of the silane. The amine group is generally unaffected by the grafting to the zeolite. Sulfur functionalization is usually done using a mercaptosilane, such as 3-mercaptoproplytrimethoxysilane. Mercaptosilanes tend to give thiol groups after functionalization. These functional groups can be oxidized to sulfonic acid functionality.

Another type of functionalization is transition metal functionalization or metal nanoparticle functionalization. Many different types of metals, such as transition metals like V, Fe, Cu and Ce have been studied in the past. Metal oxides also have been known

to be incorporated into zeolites. One type of metal oxide with desirable properties is iron oxide. Some forms of iron oxide are goethite, hematite, maghemite-Figure 1.4 and magnetite-Figure 1.5.

These oxides have different crystal structures and different ratios of iron to oxygen. Magnetite (Fe_3O_4) composites with zeolites have been shown to adsorb various pollutants, and can be easily removed from solution with a magnet. Facile removal of the zeolite adsorbents that does not require complicated equipment and trained personnel is desirable. Oliveira and coworkers developed a method for synthesizing iron oxide/zeolite magnetic composites[16]. The iron oxide/zeolite Y composites were effective adsorbents for contaminants, such as Cr^{6+}, Cu^{2+} and Zn^{2+}, from water and were also magnetic, thus facilitating easy removal from aqueous solution using a permanent magnet.

Properties can be further tailored by localization of the functional groups. Larger structures can be functionalized selectively. Different functional groups, such as metal and organic groups, can be put on different parts of the material, allowing for tailoring of the properties for different applications. Functionalization can be used to take advantage of known interactions. Some examples are amine binding to copper, sulfur binding to lead or gold and electrostatic interactions between positively charged surfaces and negatively charged anions, or between long chain n-alkylsilanes and hydrophobic organic contaminants. The different properties of the functional groups are used for reactions, and the reactions can be localized and controlled by processes such as bifunctionalization-putting two different functional groups in two different places on the zeolite, or by making larger structures with the zeolites and functionalizing various parts.

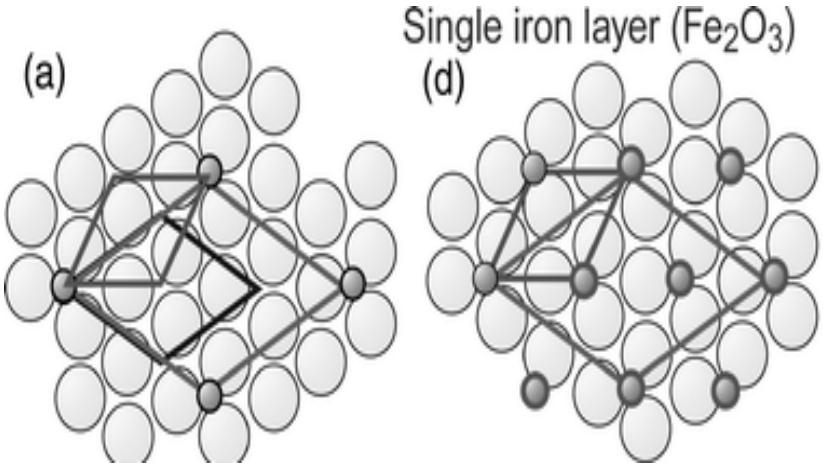

Figure 1.4 Maghemite crystal structure

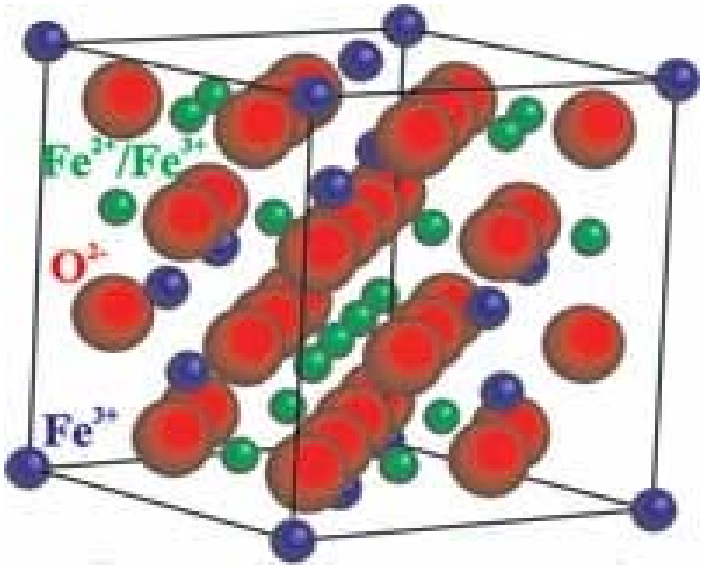

Figure 1.5 Magnetite crystal structure, with Fe^{2+} and Fe^{3+}

1.3 Adsorption of Environmental Contaminants

The porous nature of zeolites makes them good adsorbents. The walls can interact with other materials causing strong reactions. The pore system gives them a

relatively large and accessible internal surface area. This surface area can be used for a variety of purposes, and the surface can be made more reactive by the above described functionalization. Reactivity can also be tailored to specific pollutants, such as heavy metals as described on the following pages or organic farm fertilizers or other inorganic ions as needed. Reactivity can also be tailored by controlling the amount or location of the functional groups.

1.3.1 Chromium (VI)

Chromium (VI) is an environmental contaminant of importance due to its toxicity to both plants and animals. The EPA strictly regulates its presence in drinking water around the country and it is found in industrial waste effluents (electroplating, tannery and textile).[17] Removal is important for health and safety. Techniques for removal include adsorption, which is cheap and relatively easy[18-20]. However, adsorption is limited by the adsorption capacity of possible materials. Activated carbon and a variety of natural materials have been used for this purpose.

The increased external surface of nanocrystalline zeolites provides a new surface available for adsorption and reaction of molecules. Since the external surface accounts for up to 30% of the total surface area, using this surface as a reactive or absorptive surface has the potential to be valuable in applications of these materials as sorbents or catalysts or in new applications, such as drug delivery. Through surface functionalization, the properties of the zeolite external surface can be tailored for specific applications. For example, the hydrophobicity of the external surface of the zeolite can be increased through functionalization with long chain hydrocarbons, such as octylmethytrichlorosilane. Similarly, specific functional groups, sulfonic acid groups (–

SO_3H) or amine groups ($–NH_3$) can be placed on the external surface to promote acid catalyzed reactions or adsorption of DNA, respectively.

1.3.2 Arsenic

Arsenic occurs naturally in rocks and soil, water, air, and plants and animals. It can be further released into the environment through natural activities such as volcanic action, erosion of rocks and forest fires, or through human actions. Approximately 90 percent of industrial arsenic in the U.S. is currently used as a wood preservative, but arsenic is also used in paints, dyes, metals, drugs, soaps and semi-conductors. High arsenic levels can also come from certain fertilizers and animal feeding operations. Industry practices such as copper smelting, mining and coal burning also contribute to arsenic in our environment.[21]

Arsenic is a large problem in groundwater in Bangladesh and other places in the world. The current recommended exposure level by the World Health Organization (WHO) and the legal requirements in the US is 10 ppb.[22] The ideal level for health is believed to be even lower than this value, however measuring much lower concentrations can be difficult at best, and 10 ppb is the provisional limit. Many natural sources in the US and other parts of the world give levels of above 50 ppb. Some examples of places with high As levels include Bangledesh, western US sates and parts of the midwest in the US. Arsenic exposure can cause a variety of mental and physical symptoms, including cancer, neurological problems and death. [23]

Arsenic binds with sulfhydryl groups and disrupts sulfhydryl-containing enzymes; As (III) is particularly potent in this regard[24]. As a result of critical enzyme effects, there is inhibition of the pyruvate and succinate oxidation pathways and the tricarboxylic

acid cycle, impaired gluconeogenesis, and reduced oxidative phosphorylation. Another mechanism involves substitution of As (V) for phosphorus in many biochemical reactions. Replacing the stable phosphorus anion in phosphate with the less stable As (V) anion leads to rapid hydrolysis of high-energy bonds in compounds such as ATP. This leads to loss of high-energy phosphate bonds and effectively "uncouples" oxidative phosphorylation.[25]

Natural arsenic takes many forms, including H_3AsO_4 $H_2AsO_4^{-1}$, $HASO_4^{-2}$, and H_2AsO_3[26]. Arsenate, H_2AsO_3 is the most mobile and hardest to remove. Arsenic speciation depends on the rocks present, as well as the oxidization capacity of the system. Arsenate is more prevalent in oxygenated water at the surface, while arsenite(V) is less so than As (III), and generally causes damage through reduction to As (III). Because the species interconvert, techniques for remediation have to be effective for both species, and separation is difficult[22]. Because most As species are anionic at some pH, similar techniques used in chromium removal can be used for removal of this pollutant. Removal at neutral pH is desirable as the point of removal for As is more likely to be in the home, at the site of use rather than at the site of pollution[22].

Different techniques for removing arsenic have mainly involved sorbents and filters. Coagulation, reverse osmosis and activated charcoal are current technologies used. Recent activity has lead to commercially available filters, but the problem of recycling and what has to be done with the waste remains. According to the World Health Organization, simple techniques for household removal of As from water are few and have to be adapted and modified for different settings[25]. Iron has shown particular

activity related to arsenic. Some novel techniques to deal with this include Fe (VI) filters, which reduce and then coagulate the As (V).

1.4 Thesis Overview

The goal of this research is to prepare zeolites with functionalities that are chosen to promote adsorption of environmental pollutants. One part of the work focuses on synthesis of functionalized zeolite crystals, and bifunctionalized zeolite composites that can be tailored for a variety of uses. The materials were characterized by a wide range of methods to understand all properties that could be useful for future applications. In this work, zeolites are functionalized with aminopropyltriethoxysilane, and given amine functionalization, as well as functionalized with iron oxide particles to form a magnetic composite material. These functionalized zeolites and zeolite composites were used to adsorb two heavy metal environmental pollutants, aqueous chromate and arsenic. Experimental parameters were varied to understand the conditions and processing required for maximum adsorption capacity. The synthesis and functionalization of silicalite-1 crystals is discussed in Chapter 2, while the synthesis and functionalization of the iron oxide/zeolite composites will be discussed in Chapter 3. Chapters 4 and 5 focus on environmental applications of the zeolites. Chromate adsorption will be investigated in Chapter 4 and arsenate adsorption in Chapter 5. The conclusions and future directions for research will be discussed in Chapter 6.

CHAPTER 2: SYNTHESIS, CHARACTERIZATION AND FUNCTIONALIZATION OF SILICALITE-1

2.1 Introduction

Nanocrystalline zeolites have crystal sizes of less than 100 nm and very large external and internal surface areas[3, 4, 27]. A nanocrystalline zeolite with a crystal size of 50 nm has an external surface area of >100 m^2/g. For comparison, a 500 nm zeolite crystal has less than 10 m^2/g of external surface area. The increased external surface of nanocrystalline zeolites results in enhanced adsorptive properties and additional surface area available for adsorption and reaction of molecules. In principle, bifunctional nanocrystalline zeolites may be obtained by incorporating one functionality into the internal zeolite surface and a second functionality onto the external zeolite surface.

Through surface functionalization, the properties of the nanocrystalline zeolite external surface can be tailored for specific applications[13, 14, 28-30]. For example, the hydrophobicity of the external surface of the zeolite can be increased through functionalization with long chain hydrocarbons, such as octylmethyltrichlorosilane[29]. Similarly, specific functional groups, sulfonic acid groups ($–SO_3H$) or amine groups ($–NH_2$) can be placed on the external surface to promote acid catalyzed reactions or adsorption of DNA, respectively. The objective of the work described here is to functionalize and characterize the external nanocrystalline zeolite surface with various functional groups.

Methods used for functionalization of silanol groups in silica based materials, such as mesoporous silica[12, 31-33], can be readily adapted for zeolites with the main difference being that the functionalization occurs exclusively on the external zeolite

surface due to the zeolite pore sizes that restrict access to the internal zeolite surface for most organosilane reactants[14, 28]. The advantage of nanocrystalline zeolites in this regard is the extremely high external surface area relative to micron-sized zeolites. The reaction of a surface silanol group on the zeolite external surface with 3-aminopropyl triethoxysilane (APTES) results in an amine-functionalized zeolite as shown schematically in Figure 2.1. This method is versatile because many different organosilane reagents can be used to introduce different functionalities to the zeolite surface, giving many different possible properties to the final material.

Recently, there have been several studies of chromate adsorption on amine-functionalized mesoporous silica (MCM-41 and SBA-15)[19, 20] and studies of chromate adsorption on organic functionalized natural zeolites[13]. Surface modification is accomplished through reaction of surface silanol groups with organosilane reagents. This strategy has been widely adopted to functionalize mesoporous silica materials with catalytically active or biologically compatible functional groups such as sulfonic acid or antibodies. SBA-15 and MCM-41 have been functionalized with amine functional groups using organosilanes, such as amino-propyltriethoxysilane (APTES)[34].

Silicalite is the purely siliceous form of the zeolite, ZSM-5 which has the MFI structure with 5.6 Å pore diameter. In this study, nanocrystalline silicalite with a crystal size of 32 nm and an external surface area of 100 m^2/g was functionalized with varying amounts of APTES so that the surface properties (such as zeta potential) could be systematically varied and tailored for chromate adsorption. The same techniques described above to functionalize mesoporous silica materials were applied here to these silicalite nanocrystals.

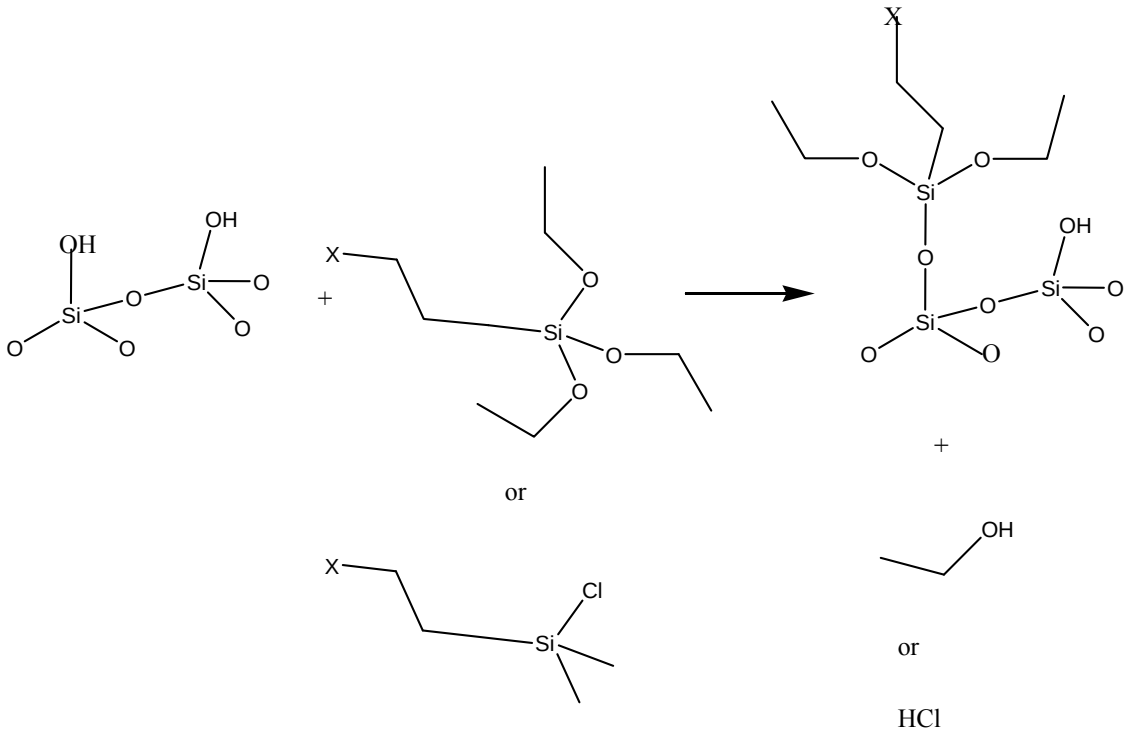

Figure 2.1 Silicalite-1 functionalization scheme, shown here for a general case.

The functionalized silicalite was characterized by powder X-ray diffraction, ^{29}Si magic angle spinning (MAS) NMR, thermal gravimetric analysis (TGA), nitrogen adsorption isotherms and zeta potential measurements

Zeolite functionalization can also be applied to larger zeolite structures. Several crystals can be formed into one overall shape, such as a hollow tube[35]. These structures can be functionalized all over, or can be selectively functionalized by functionalizing only one surface of the structure. The two methods for doing so include making the tubes out of functionalized material, as shown in Figure 2.2 and functionalizing the material after the tubes are made. In this chapter, the synthesis, characterization and functionalization of nanoscale silicalite-1 and hollow silicalite structures will be described.

2.2 Synthesis of Silicalite-1

A silicalite-1 sample with a crystal size of 32 nm was synthesized according to the method described previously[9], via a synthesis gel composed of a ratio of (495:25:9:0.16) moles of H_2O:tetrapropyl ammonium hydroxide(TPAOH):tetraethyl orthosilicate(TEOS) to NaOH heated to 65°C for 5 days. The external surface area of the uncalcined silicalite-32 nm was 99 m^2/g.

2.2.1 Synthesis of Silicalite Hollow Tubes

Silicalite tubes were prepared by synthesizing a mesoporous silica template material-MCM-4. To make the hollow zeolite structures 0.5 g MCM-41 was coated with polydiallyldimethylammoniumchloride (2% solution-PDDA) and washed with a pH 10 NH_4OH solution. The resulting solids were coated with an as synthesized colloidal (particle size around 30 nm) silicalite solution and aged for 20 min at room temperature.

The solids were then washed again with NH_4OH solution. After drying at 60 °C for 2 h., the solids were suspended in an autoclave above 1 mL ethylenediamine, 30 mL diethylamine and 5 mL water and heated to 160 ° for 7 days, then washed with water and dried at 60°C. A visual scheme of this process is seen in Figure 2.2

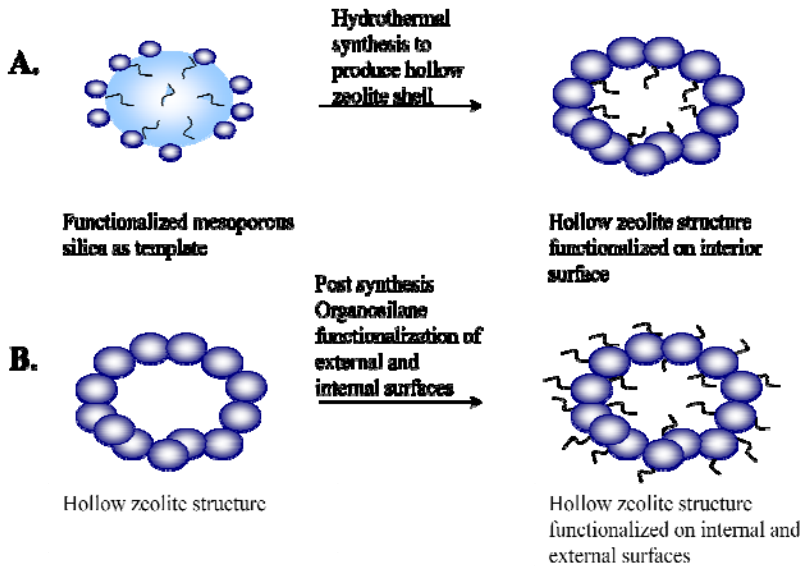

Figure 2.2 Scheme for making hollow tubes and functionalized hollow zeolite tubes

2.3 Functionalization of Silicalite-1

2.3.1 APTES Functionalization Procedure

To functionalize the silicalite, 0.5 g of calcined silicalite (32 nm) was added to 60 mL toluene and 0.25 0.5, 1.0 mL aminopropyltriethoxysilane (APTES). The reaction mixture was heated to 383K for 4 h and then was centrifuged. The solids were washed

with water and ethanol and dried overnight at 368K a visual representation can be seen in Figure 2.1

2.3.2 MCM-41 Functionalization With MPTMS

The MCM-41 template was functionalized prior to the synthesis of the hollow zeolite structures. 1g of MCM-41 was added to 150 mL toluene and 4.1g mercaptopropyltrimethylsilane (MPTMS) and heated to 90°C in an oil bath for 24 h resulting in pink S-H functionalized MCM-41. To form sulfonic acid functionality, the solids were collected by centrifugation and then dissolved at room temperature in a 3:1 methanol H_2O_2 for 24 h. The solids were washed with EtOH/CH_2Cl2_2 and dissolved in 1% H_2SO_4 for 4 h at room temperature to make functionalized MCM-41.

The resulting functionalized MCM-41 could be used as the template for the interior functionalized zeolite tubes. The functionalized MCM-41 was coated with PDDA as described above and coated with silicalite seed crystals and washed and heated in the autoclave as described previously

2.3.3 MCM-41 Functionalization With APTES

The MCM-41 template was functionalized prior to the synthesis of the hollow zeolite structures. 1g of MCM-41 was added to 50 mL toluene and 2mL Aminopropyltriethoxysilane (APTES) and heated to 90°C in an oil bath for 24 h then washed with water and dried at 95°C overnight resulting in APTES functionalized MCM-41.

The resulting functionalized MCM-41 could be used as the template for the interior functionalized zeolite tubes. The functionalized MCM-41 was coated with

PDDA as described above and coated with silicalite seed crystals and washed and heated in the autoclave as described previously

2.4 Characterization

Powder XRD patterns were obtained using a Siemens D5000 diffractometer with Cu Ka target and a nickel filter. XRD patterns were collected between 2θ 5°and 35°. ^{29}Si MAS NMR was conducted using a 300 MHz wide bore magnet with a TecMag Discovery console and a Chemagnetics double-channel 7.5 mm pencil MAS probe (59.6 MHz). 1000 scans were collected with a 60 s pulse delay and a spinning speed of 6 kHz. Thermogravimetric analysis was performed on a TA Instruments Q500 TGA by heating from room temperature at 5.00 °C/min to 1000 °C under N_2. The results were analyzed using TA Universal Analysis Software with the amine peak appearing at approximately 300°C-600°C. Zeta potential measurements were obtained using a Malvern Zetasizer Nano. The zeta potential was measured using a 1–2% by weight suspension of the zeolites in deionized water. The samples were sonicated for 60 min prior to the zeta potential measurements and placed in disposable zeta potential cells. Nitrogen adsorption isotherms were obtained on a Quantachrome Nova 4200e multipoint BET apparatus using approximately 0.1 g of sample for each measurement. Prior to the N_2 adsorption, each sample was vacuum degassed at 373K for 2–3 h. The specific surface area was calculated by the BET method using the Nova 4200e instrument software.

2.5 Results and Discussion

2.5.1 Synthesis and Characterization of Nanocrystalline Silicalite-1

Nanocrystalline silicalite with a crystal size of approximately 32 nm was synthesized and characterized. The external and total surface areas of the silicalite-32 nm

were 99 m^2/g and 444 m^2/g, respectively. The crystal size was calculated from the external surface area: $S_{ext} = 3214/x$ where S_{ext} is the external surface area in m^2/g and *x* is the silicalite-1 crystal size in nm, as described previously[9]. The silicalite-32 nm was functionalized with varying amounts of APTES (0.25, 0.5 and 1.0 mL) to achieve systematically varied surface functionalization. TGA was used to quantify functionalization, as show in Table 2.1

The extent of functionalization was characterized by ^{29}Si MAS NMR as shown in Figure 2.3. A framework silicon peak is observed at –113 ppm and a second peak attributed to the silicon atom from the APTES is observed at ~ -65 ppm for amine functionalized silicalite-1. The intensity of the -65 ppm is proportional to the amount of functionalization of the zeolite surface and can be seen to increase with increasing APTES concentration in Figure 2.3. The APTES functionalization can be quantified through integration of the ^{29}Si MAS NMR peaks. The percent functionalization is calculated from the ratio of the integrated area of the -65 ppm peak to the sum of the integrated areas of the peaks at -113 and -65 ppm. The results are provided in Table 2.1. The % functionalization increases as expected with the increase in the APTES concentration.

The XRD powder pattern, characteristic of the MFI zeolite structure, did not change as a result of functionalization as shown in Figure 2.3 indicating that the zeolite structure remains intact after functionalization. Neither amine nor thiol functionalization altered the crystal pattern, as shown by comparing Figure 2.3a to the unfunctionalized zeolite in 2.3b to 2.3c. Crystallinity was not affected by the functionalization procedure for the silicalite-1 crystals.

The BET surface area was measured by nitrogen adsorption for each of the functionalized silicalite samples (Table 2.1) and the total specific surface area decreased as the extent of functionalization increased. The surface functionalization causes a dramatic decrease in the surface area suggesting that access to the internal zeolite surface is blocked by the functional groups. This suggests that functionalization may occur to a large extent at the zeolite pore mouth thus restricting access to the zeolite pores.

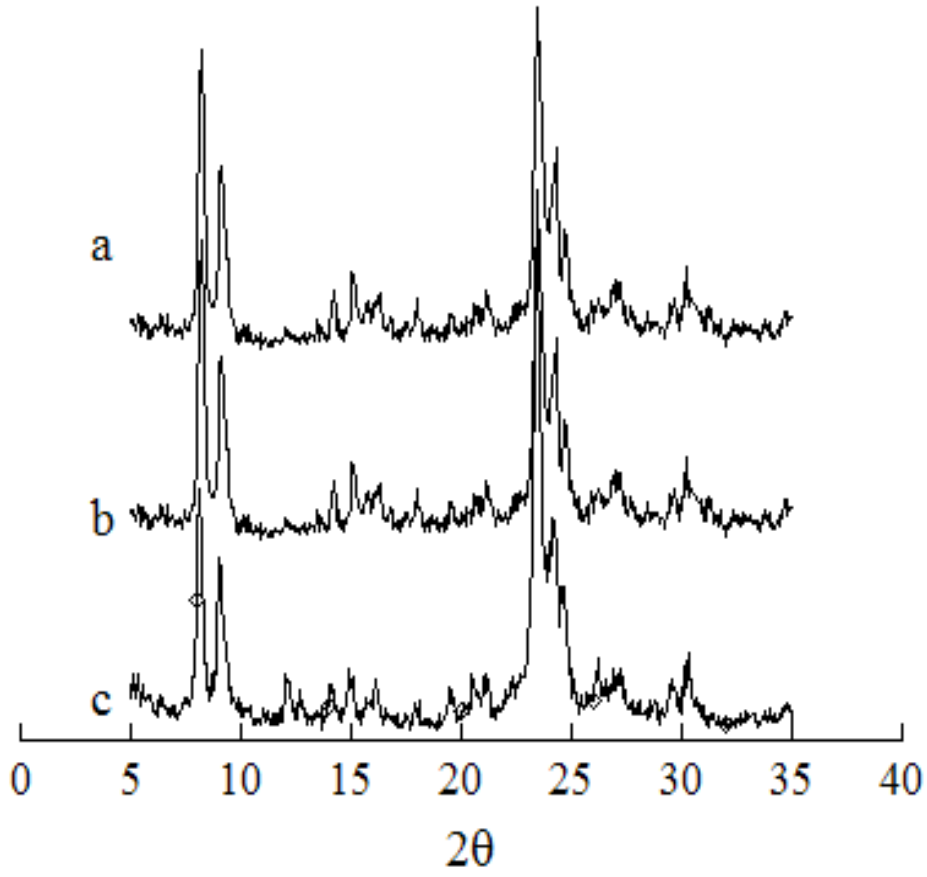

Figure 2.3 Powder XRD patterns for a)amine functionalization, b)thiol functionalization and c)unfunctionalized nanocrystalline silicalite samples

The relationship between APTES concentration and the surface area is graphed in Figure 2.4. The surface area decreases and is asymptotically leveling off at ~100 m^2/g which is approximately equivalent to the external surface area of the parent silicalite. The relationship between surface area and extent of functionalization supports the hypothesis that the functionalization occurs near the zeolite pore mouth blocking access to the internal surface. The zeta potential for the silicalite and APTES functionalized silicalite in water was measured at pH~5 and the results are listed in Table 2.1. The zeta potential represents the surface charge and varies with pH and ionic strength[36]. The zeta potential of unfunctionalized silicalite reflects the protonation of surface hydroxyl groups according to the following equilibrium:

$$SiOH_2^+ \underset{+H^+}{\overset{-H^+}{\rightleftharpoons}} SiOH \underset{+H^+}{\overset{-H^+}{\rightleftharpoons}} SiO^- \qquad (1)$$

The zeta potential for APTES functionalized silicalite is governed by the following equilibrium involving the protonation of the surface amino groups: The pKa for the second part of (1) is 9 amd 4-5 for the first part, implying that at all pHs studied the groups will be protonated in some form and will be in the form of SiOH for pH above 4-5, and $SiOH_2^+$ below that at pH 2. The amine groups have a pKa of around 9 and are expected to be protonated at all pHs under study.

$$SiOSi(OCH_2CH_3)_2 - C_3H_6NH_2 \underset{+H^+}{\overset{-H^+}{\rightleftharpoons}} SiOSi(OCH_2CH_3)_2 - C_3H_6NH_3^+ \quad (2)$$

The zeta potential (at pH=5) for the parent silicalite was -41 mV indicating that the surface silanol groups are deprotonated to SiO^- as indicated in equation 1. The zeta potential (at pH=5) increased to -26, -15 and -3.4 mV as the APTES functionalization increased as shown in Table 2.1. The increase in zeta potential with APTES

functionalization is attributed to an increase in the functionalization of the silanol groups on the zeolite surface (equation 2). The zeta potential appears to level off as it approaches 0 mV suggesting that all of the surface silanols have been functionalized with APTES. When the pH is decreased, the zeta potential increases as the amino group is protonated. For silicalite-30 nm functionalized with 0.5 mL of APTES, the zeta potential increases from -15 mV at pH=5 to +14 mV at pH=2, as expected based on equation 2. Zeta potential, functionalization and surface area are all related to the amount of functionalization, and show inverse and direct relationships respectively, as seen in Figure 2.4 As the amount of silane added increases, the surface area decreases, to almost the external surface area of 99 m^2/g when 1 mL of silane is added.

Table 2.1.Physicochemical Properties of Functionalized Silicalite-32 nm

Sample	Functionalization (volume)	%Si Functionalized [a]	Surface Area[b] (m^2/g)	Zeta potential[c] (mV)
Silicalite-32 nm	None	NA	444	-41
Silicalite-32 nm .25	APTES (0.25 mL)	<1%	218	-26
Silicalite-32 nm .5	APTES (0.5 mL)	2	141	-15
Silicalite-32 nm 1	APTES (1.0 mL)	4	121	-3.4

[a]Determined from ^{29}Si MAS NMR

[b] Total specific surface area measured by nitrogen adsorption and the BET method

[c] solution pH~5

As more silane was added, the zeta potential increased from -41 to -3 mV. This increase is consistent with a protonated amine group. The mmol/g of 0.31 gives 1.9 amine groups/nm^2, only half the number of groups cited by literature[37, 38]. The possibility of increased functionalization is there, though extra alkoxy groups on APTES could cross react with neighboring silanol sites, reducing the possibility for new functionalization. XPS is not quantitative, so thiol groups were not able to be quantified. The blockage of the surface pores drastically reduces the available surface area, a possible area of concern for adsorption and other reactions, which will be investigated in later chapters. The log of the surface area was plotted as a function of Zeta potential to look for linear trends in the relationship. The plot fit with a line with the equation y=1.9757-.015, R=.975

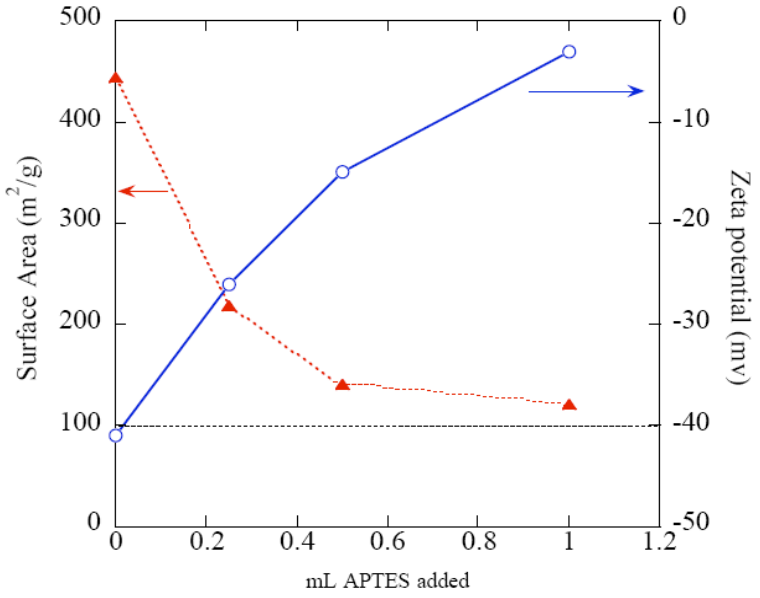

Figure 2.4 Graph showing the relationship between physicochemical properties and APTES added

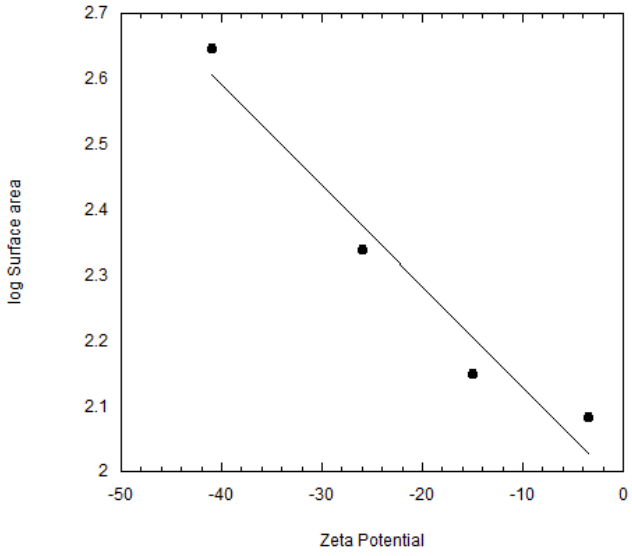

Figure 2.5-Graph showing the relationship between log surface area and zeta potential

2.5.2 Amine and Sulfur Functionalization of Hollow Silicalite Tubes

Hollow silicalite tubes were synthesized, characterized and then functionalized with both amine and sulfur groups. The sulfur functionalization was then oxidized to sulfonic acid functionality. Different functional groups provided very similar ^{29}Si MAS NMR peaks. Figure 2.3 shows the XRD patterns for both amine functionalized silicalite-1 in Figure 2.3a and thiol functionalized zeolites in Figure 2.3b. ^{29}Si MAS NMR is used to probe the silicon environment. Both silanes-APTES and MPTMS have silicon attached to a propyl organic chain. The peaks are both observed around -63 ppm and are very small in comparison to the framework silicon peak. While other methods can characterize the difference between functional groups, ^{29}Si MAS NMR cannot. Surface areas for tubes tend to be extremely small-50 m^2/g even when they are unfunctionalized. Amine functionalization lowered this only slightly, down to 44 m^2/g. Thiol

functionalization also lowers the surface area to 41 m^2/g. Thiol functionalization blocks the pores even more than the APTES functionalization, giving a surface area of just 45 m^2/g, down from 444 m^2/g.

^{29}Si MAS NMR for APTES and MPTMS functionalized silicalite hollow tubes are shown in Figure 2.6 and 2.7. The amine MCM-41 shows a large peak at 64ppm, indicating a high level of functionalization of the MCM-41. The hollow silicalite tubes show a peak in the same range, though smaller. Thiol tubes showed a functionalization peak at-63 ppm in the same area as the amine peak. The similarity of silicon environments between the silanes that lead to similar functional groups in the crystals lead to a similar functionalization peak in the tubes. In both cases the silicon atom in the silane was bonded to a propyl group, leading to a similar chemical shift.

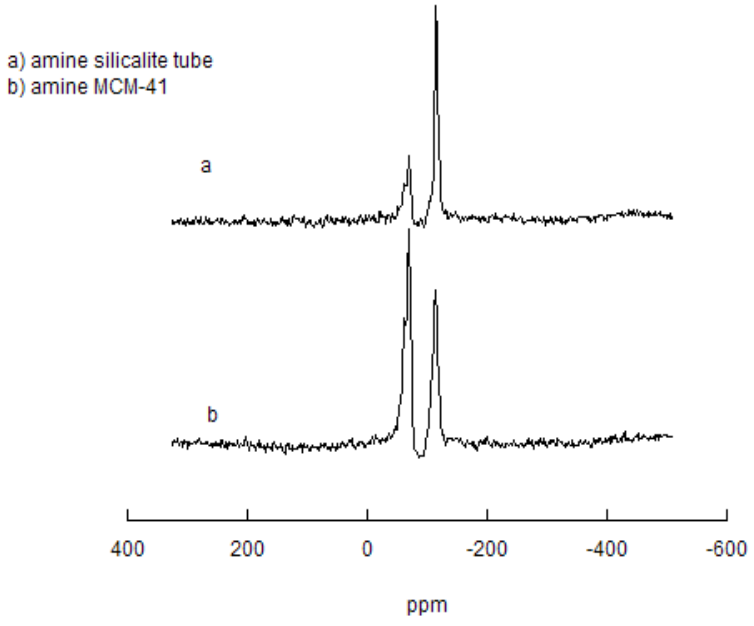

Figure 2.6 ^{29}Si MAS NMR spectra for a) amine functionalized tubes and b) MCM-41 tubes.

XPS can be used to probe the sulfur in the thiol and sulfonic functionalized tubes. Thiol functionalization was monitored by X-ray photoelectron spectrography of the 2p electrons as seen in Figure 2.8. The peak was observed at 165 eV before oxidation- consistent with reduced sulfur. After oxidation two smaller peaks are seen, one remaining at 165 eV and a second peak at 168 eV that represents half the sulfur in the sulfonic acid functionalized hollow tubes.

Thiol functionalization does not change the zeta potential as much-the surface charge is 6mV. When the functionalization occurs, as it is not a charged surface group. When the thiol is oxidized to sulfonic acid, the charge increases to +35mV. The sulfonic acid functionality is expected to be protonated at pH 5, explaining the highly positive surface charge measured.

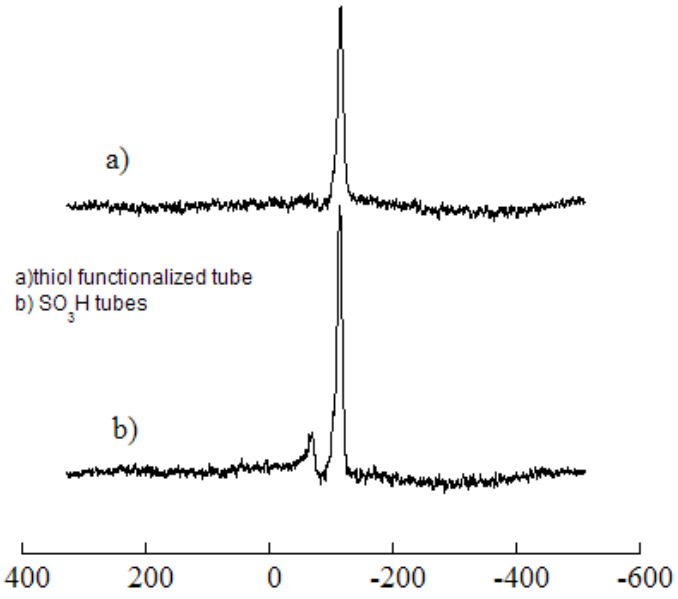

Figure 2.7 ^{29}Si MAS NMR results for a)thiol functionalized silicalite-1 tubes and b) SO_3H oxidation

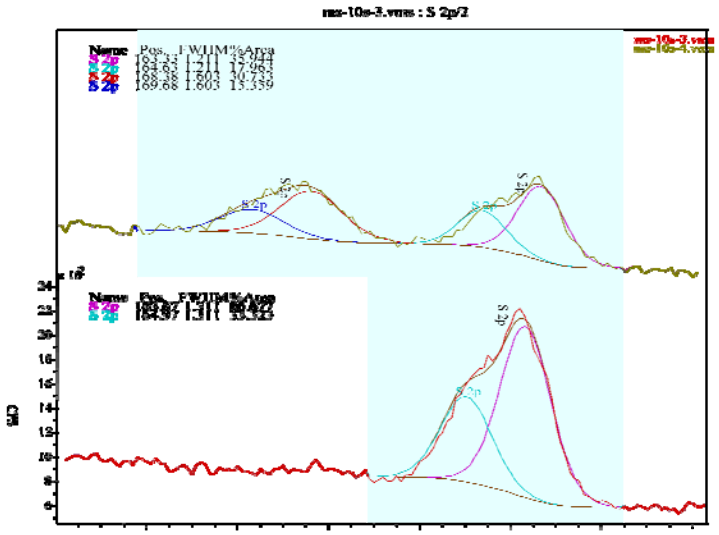

Figure 2.8 Sulfur 2p XPS of sulfur functionalized silicalite-1 tubes, before acidification on the bottom, and after acidification on the top

2.6 Conclusions

Nanocrystalline silicalite and hollow silicalite tubes were functionalized with organosilanes. Nanocrystalline silicalite with a size of approximately 30 nm was systematically functionalized with varying amounts of APTES. The APTES functionalized silicalite was characterized by powder XRD, solid state ^{29}Si MAS NMR TGA and zeta potential. The trend of decreasing surface area and zeta potential with increasing APTES functionalization was observed. These results demonstrate that the external of nanocrystalline zeolites can be tailored through functionalization in order to achieve desired results. Hollow silicalite tubes were functionalized with APTES or MPTMS. ^{29}Si MAS NMR and XPS were used to characterize the resulting sulfur functional groups. Nanocrystalline silicalite with a crystal size of 32 nm was functionalized with varying amounts of APTES and chromate adsorption was measured.

The adsorptive properties of the functionalized silicalite for chromate will be discussed in Chapter 4.

CHAPTER 3: SYNTHESIS, FUNCTIONALIZATION AND CHARACTERIZATION OF IRON OXIDE/ZEOLITE COMPOSITES

3.1 Introduction

Iron oxide zeolite Y composites with surface amine groups and magnetic properties were synthesized. As described in Chapter 2, nanocrystalline silicalite with a size of approximately 30 nm was systematically functionalized with varying amounts of APTES. The APTES functionalized silicalite was characterized by powder XRD, solid state ^{29}Si MAS NMR TGA and zeta potential. The trend of decreasing surface area and zeta potential with increasing APTES functionalization was observed. These results demonstrate that the external of nanocrystalline zeolites can be tailored through functionalization in order to achieve desired results. Building on the previous results, zeolite composites with magnetic iron oxide in the form of maghemite (γ-Fe_2O_3) were synthesized from Y zeolites using a Fe^{2+}-Fe^{3+} ion mixture and were subsequently functionalized with 3-aminopropyltriethoxysilane (APTES) to form bifunctional zeolite composites. The amine functionalized iron oxide/zeolite composites were characterized by powder X-ray diffraction to verify crystallinity, thermal gravimetric analysis to quantify the functionalization and zeta potential measurements to monitor surface charge. The iron oxide phase was assigned to maghemite based on X-ray photoelectron spectroscopy and Mössbauer spectroscopy. The APTES functionalization increased the zeta potential and this lead to increased chromate adsorption relative to unfunctionalized iron oxide/zeolite composites. Recovery of the iron oxide/zeolite composite from aqueous solution can be accomplished using the magnetic properties of the material. The

methods for preparation amine functionalized nanocrystalline zeolites were presented in Chapter 2 and are used here as well.

Amine functionalized zeolites dispersed in water can lead to a strongly dispersed colloidal solution in water making it extremely difficult to recover the adsorbent material. Facile removal of the zeolite adsorbents that does not require complicated equipment and trained personnel is desirable. Oliveira and coworkers developed a method for synthesizing iron oxide/zeolite magnetic composites.[39, 40] The iron oxide/zeolite Y composites were effective adsorbents for contaminants, such as Cr^{6+}, Cu^{2+} and Zn^{2+}, from water and were also magnetic, thus facilitating easy removal from aqueous solution using a permanent magnet. Other groups have reported the preparation of magnetic zeolites for seawater purification[41] and biomedical applications[27, 28]. The preparation of magnetic mesoporous silica materials for use as magnetic adsorbents [42] and for biomedical applications[29-31] has also been reported. Recently, Yeung and coworkers have reported the preparation of a magnetic mesoporous adsorbent with grafted amine groups that is an effective adsorbent for chromium (VI) and arsenic (V).

In this study, magnetic iron oxide/zeolite Y composites were prepared and were then functionalized with amine groups to form a bifunctional, magnetic zeolite. The objective is to prepare a functionalized zeolite material that has enhanced adsorptive properties for chromate, combined with facile recovery of the adsorbent via the magnetic iron oxide component of the composite material. The iron oxide/zeolite Y composite was amine functionalized using 3-aminopropyltriethoxysilane (APTES) as described previously for zeolites and mesoporous silica materials.[12, 17, 22, 24, 32, 33] The physicochemical properties of the composite zeolite materials were investigated using

powder X-ray diffraction (XRD), nitrogen adsorption isotherms (BET method), inductively coupled plasma optical emission spectroscopy (ICP-OES), zeta potential measurements, thermal gravimetric analysis (TGA), Mössbauer spectroscopy and X-ray photoelectron spectroscopy (XPS). The chromate adsorption as a function of pH was studied and will be presented in chapter 4.

3.2 Synthesis of Iron Oxide/Zeolite Composites

Nanocrystalline NaY (Y-nano) with a size of approximately 79 nm and Si/Al=1.9 was synthesized according to a previously published procedure.[28] NaY from Zeolyst (Si/Al=2) was also used in these studies. Textural properties of NaY (Zeolyst and Y-nano) are provided in Table 3.1. To convert the sodium form of the zeolite into the H-form, NaY (Zeolyst or Y-nano) was added to 1.0 M NH_4NO_3, stirred overnight, and then calcined in air at 550°C for 12 h. Following the procedure of Oliveira and co-workers[39], iron oxide/Y composites were formed. HY (Zeolyst or nano) was added to 200 mL of nitrogen purged water and then 30 mL of a 1:2 mol ratio of $FeCl_3$:$FeSO_4$ was added dropwise in a glove bag under nitrogen. The resulting iron oxide/zeolite composite will be designated *iron oxide/Y-Zeolyst* or *iron oxide /Y-nano*. The composite materials were washed with water and ethanol, dried in an oven overnight at 368 K, and then annealed under N_2 for 6 h. at 723K.

3.3 Functionalization of Composites With APTES

After annealing, the iron oxide/zeolite material was functionalized with aminopropyltriethoxysilane (APTES) according to literature procedures as discussed in chapter 2.[43] 0.5 g of iron oxide/zeolite composite (or zeolite Y) was refluxed in 50 mL toluene and 1.5 mL APTES for 4.5 h. The samples were washed with water and

ethanol and dried at room temperature overnight. These APTES functionalized samples are designated as *Y-nano-APTES*, *Y-Zeolyst-APTES, iron oxide/Y-nano-APTES and iron oxide/Y-Zeolyst-APTES.*

3.4 Characterization

The zeolite and zeolite composite samples were characterized by powder X-ray diffraction (XRD), nitrogen adsorption isotherms (BET method), inductively coupled plasma optical emission spectroscopy (ICP-OES), zeta potential measurements, thermal gravimetric analysis (TGA), Mössbauer spectroscopy and X-ray photoelectron spectroscopy (XPS).

XRD patterns were obtained using a Rigaku Mini Flex II system with a Cobalt X-ray source and a Fe K-beta filter to filter out the K-beta lines from the Co source. XRD patterns were collected between 2θ of 5 and 75 degrees with a step size of 0.04° and were analyzed with MDI Jade software. Nitrogen adsorption isotherms were obtained on a Quantachrome Nova 4200e multipoint BET apparatus using approximately 0.1g of sample for each measurement. Prior to the N_2 adsorption, each sample was vacuum degassed at 120 °C for 2–3 h. The specific surface area was calculated by the BET method using the Nova 4200e instrument software. Zeta potential measurements were obtained using a Malvern Zetasizer Nano. The zeta potential was measured using a 1–2% by weight suspension of the zeolites in deionized water. The samples were sonicated for 60 min prior to the zeta potential measurements and placed in disposable zeta potential cells.

ICP/OES analysis was conducted using a Varian 720-ES ICP/OES spectrometer. Typically, 5 mg of the sample was digested in 3 mL 70:30 HCl: HF mixture. After the

solids were allowed time to dissolve, 1 mL of concentrated nitric acid and 15 mL of 5% boric acid were added and the volume was adjusted to 25 mL with deionized water. 1 ppm solution of yttrium standard solution was used as an internal standard during the measurements. TGA was performed on a TA Instruments Q500 TGA by heating from room temperature at 5.00 °C/min to 1000 °C under N_2. The results were analyzed using TA Universal Analysis with the amine peak appearing at approximately 350 °C.

The iron oxide species were characterized using Mössbauer spectroscopy and XPS. Mössbauer spectra were collected in transmission mode with a constant acceleration drive system and a ^{57}Co source. Samples for Mössbauer spectroscopy were mounted in a top loading Janis exchange-gas cryostat. The source was maintained at room temperature during analysis. Data was calibrated against an α-Fe metal foil collected at room temperature. Spectral fitting was done with the Recoil software package. The Mössbauer spectra were compared to known spectra of superparamagnetic iron oxide materials for identification. For XPS spectroscopy, a monochromatic Al K_α X-ray source was used to scan the samples. The pressure in the analysis chamber was maintained in the range of $1.33*10^{-6}$ to $1.33*10^{-7}$ Pa. Low energy electrons were used to maintain a uniform charge on the samples. Wide energy range survey scans were acquired using following parameters: energy range from 1200 to -5 eV, pass energy of 160 eV, step size of 1 eV, dwell time 200 ms, x-ray spot size 700 x 300 mm. High resolution spectra were acquired using following parameters: energy range of 50 - 20 eV depending on the peak examined, pass energy of 20 eV, step size of 0.1 eV, dwell time of 1000 ms. Three sweeps were used for the Fe 2p region to enhance signal to noise. The spectra were fit using Shirley background Gaussian-Lorentzian(30) fitting program with

the Kratos software package in the University of Iowa Central Microscopy Research Facility.

3.5 Results and Discussion

3.5.1 Physicochemical Characterization of Iron Oxide/Zeolite Y Composites

Powder XRD was used to evaluate crystallinity and to potentially identify the different component phases of the iron oxide/zeolite materials. The powder XRD patterns of as-synthesized iron oxide [39], zeolite Y-Zeolyst and iron oxide/Y composites are shown in Figure 3.1. The reflections observed in Figure 3.1a are consistent with the iron oxide phases, maghemite (Fe_2O_3) and magnetite (Fe_3O_4), which have similar XRD powder patterns making it difficult to distinguish between these two iron oxide phases based on the XRD patterns. The lines in the Figure show database patterns for those materials maghemite and magnetite. The XRD powder pattern for the parent Y zeolite from Zeolyst is shown in Figure 3.1d for comparison with the composite materials. The XRD powder patterns of the iron oxide/zeolite composites (Figure 3.1 b,c) indicate that dominant features are the zeolite reflections with possible weak contributions from the iron oxide phase at a $2\theta \sim 42°$. The zeolite reflections are strong enough to mask the broader peaks of the iron oxide phase almost completely. The crystal structure of the zeolite patterns are not distorted by the iron oxide crystals. The XRD lines of the iron oxide/Y-nano composite (Figure 3.1b) are significantly broadened relative to the Zeolyst Y (Figure 3.1d) due to the decreased crystal size of the Y-nano.[28] This broadening has been seen in smaller crystals of other zeolites as well, such as silicalite-1.[9]

The specific surface areas of Y-Zeolyst and Y-nano were measured by nitrogen adsorption and BET analysis and are listed in Table 3.1. The external surface area for as-synthesized nanocrystalline NaY was measured with the template still in the pores of zeolite Y and was 51 m^2/g, which can be used to calculate the particle size assuming cubic crystals. The external surface area corresponds to a crystal size of 79 nm according to $x=4061/S_{ext}$ where x= crystal size in nm and S_{ext} is the external surface area.[28] This fit has been established for a variety of zeolites and gives very small error. APTES functionalized Y and the iron oxide/Y (both nano and Zeolyst) composites exhibited a decrease in specific surface area after functionalization or iron loading (Table 3.1). The decrease of surface area is due to blocking of the zeolite pores by the iron oxide species and/or functional groups and has been observed previously for related materials [1, 10, 12]. Pore blocking leads to restricted access to the internal zeolite surface. The BET surface areas for the iron oxide/Y-Zeolyst-APTES and iron oxide/Y-nano-APTES composites were quite small, 50 and 25 m^2/g, respectively. The iron oxide is not a porous material; as such the composites cannot have the same surface area as the zeolites. Amine functionalization heightens this effect, and the surface area is further decreased.

The APTES loading was determined by TGA analysis and the results are listed in Table 3.1. 0.65 and 0.55 mmol/g APTES was grafted onto iron oxide/Y-Zeolyst and iron oxide/Y- nano, respectively.

The weight percentages of iron in the iron oxide/zeolite composites were determined by ICP/OES to be 19 and 18%, respectively, for iron oxide/Y-Zeolyst and iron oxide/Y-nano. The zeta potential varies with pH and ionic strength and represents

the surface charge. [36] The zeta potential for the Zeolyst Y and nano-Y and the iron oxide / zeolite composites at pH=7 are listed in Table 3.1.

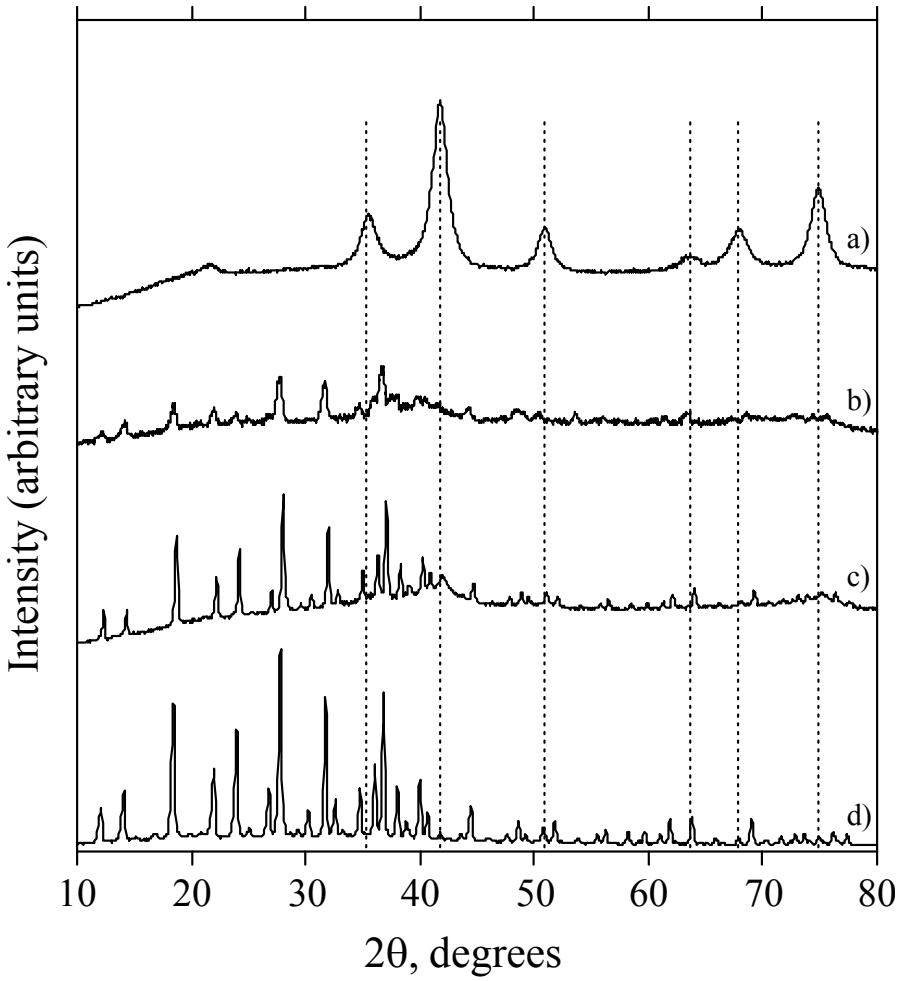

Figure 3.1. Powder XRD patterns for: a) iron oxide (Fe_2O_3) as synthesized, b) iron oxide/Y-nano, c) iron oxide/Y-Zeolyst and d) Y Zeolyst. The dashed lines indicate iron

Table 3.1:Physicochemical Properties of Iron Oxide/Zeolite Composites

Sample	SSA/ (m^2/g)[a]	ζ-potential (mV)[b]	APTES loading (mmol/g)[c]
Y-Zeolyst	440	-25(1.3)	--
Y-nano 79 nm	(51))	-19(1.1)	--
Iron oxide/Y-Zeolyst	120	-27(0.7)	--
Y-Zeolyst-APTES	225	-5(1.6)	0.80
Iron oxide/Y-Zeolyst-APTES	50	-4(1.8)	0.65
Iron oxide/Y-nano-APTES	25	-4(1.6)	0.55

[a] Specific surface area (SSA) was measured by nitrogen adsorption and the BET method. The external surface area is given in parenthesis.

[b]ζ-potential measured at pH=7.

[c] The APTES loading was measured using TGA.

The zeta potential of the parent Y zeolites reflects the protonation of surface hydroxyl groups according to the same equilibrium as noncomposite silicalite listed in chapter 2

The zeta potential at pH=7 was -25 mV and -19 mV for the Zeolyst and nano HY samples, respectively. When zeolite Y is functionalized with APTES, the zeta potential will change relative to the parent zeolite due to the protonation of the surface amine groups as shown in chapter 2. Functionalization of zeolite Y with APTES leads to a pH-dependent increase in the zeta potential relative to the parent zeolite. Similarly, APTES functionalization of iron oxide/Y composites leads to a similar increase in zeta potential.

Mössbauer spectra of iron oxide/Y-Zeolyst-APTES and iron oxide/Y-nano-APTES were obtained at 13 K and are shown in Figure 3.2a, b, respectively. The Mössbauer spectrum of maghemite (Fe_2O_3) is shown in Figure 3.2c for comparison. The Mössbauer spectra confirmed the presence of iron oxide and were used to identify the iron oxide species in the composite materials. The spectra were fit using the Recoil software to obtain the center splitting (CS) and the magnetic splitting (H). The fitting results for the composite samples are listed in Table 3.2 along with maghemite and magnetite standards for comparison. The iron oxide phase in the zeolite composites (Figure 3.2 a,b) was identified as primarily maghemite (Fe_2O_3), a superparamagnetic iron oxide.

Mössbauer spectra tend to have characteristic parameters for different species of iron. Figure 3.2 shows a clear sextet on all samples, comparable to the maghemite example in the bottom.

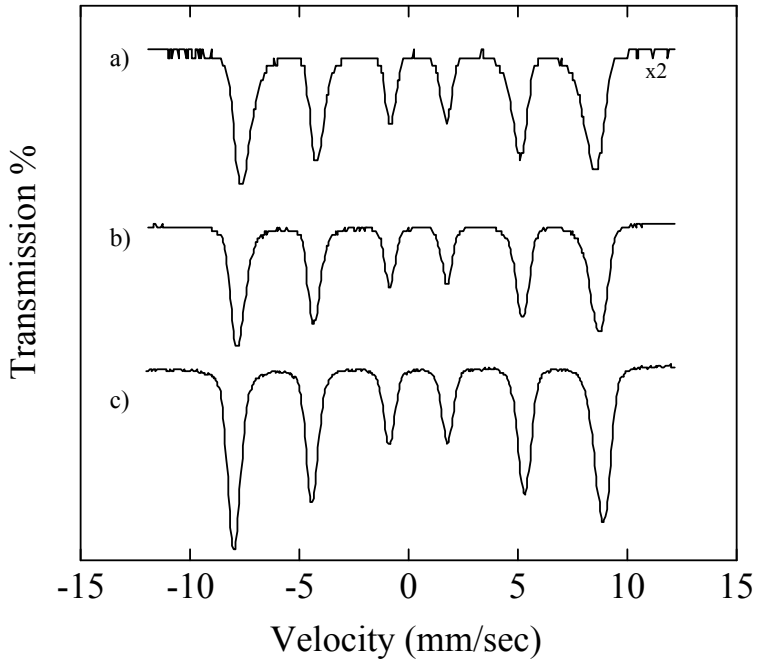

Figure 3.2. Mössbauer spectra collected at 13K for: a) iron oxide/Y-Zeolyst-APTES, b) iron oxide/Y-nano-APTES, and c) iron oxide (Fe_2O_3) standard

Table 3.2: VBF Mössbauer Parameters for Magnetic Zeolite Composites

Sample	CS (mm/s)[a]	H (T)[b]	T(K)	Reference
Iron oxide/Y-Zeolyst	0.30 0.53	48.8 50.1	12	This work
Iron oxide/Y-nano	0.31 0.57	50.8 51.3	12	This work
Maghemite	0.30 0.57	48.8 51	12	Scherer unpublished
Magnetite	0.84 0.44	50.2 52.3	12	Scherer unpublished

[a] Center shift

[b] Magnetic splitting

Neither of the zeolite iron species shows significant doublets. The iron species are made up of almost exclusive Fe (III). Samples were shown at 13K for ease of viewing, magnetic ordering takes place in samples taken at 77K The parameters and the spectra show significant Fe(III) character and not much Fe(II) character. XPS data supports this analysis.

XPS spectra of iron oxide/Y-Zeolyst-APTES and iron oxide/Y-nano-APTES obtained in the Fe 2p region are shown in Figure 3.3a, b, respectively. The Fe 2p region of the XPS spectrum is complex and often includes contributions from overlapping peaks of Fe^0, Fe^{2+} and Fe^{3+} oxides. Literature values [37-40] for binding energies for various iron oxide compounds can be found and used to interpret the XPS spectra. Fe_2O_3 (Fe^{3+}) has a binding energy of 711.1 eV (with shake-up satellite peak at 719.8 eV[44]) and FeO (Fe^{2+}) has a binding energy of 709.9 eV (with shake-up satellite peak at ~715 eV[44]). The mixed valence compound Fe_3O_4 has a binding energy ranging from 710.5 to 711.2 eV.[45] These iron oxide species have been previously observed in XPS studies of iron-exchanged zeolites [41-43].

A sharp Fe $2p_{3/2}$ peak is seen at a binding energy of ~710 eV for both the commercial and the nanosized zeolite composite samples in Figure 3.3. This peak is primarily attributed to Fe^{3+} oxide species present in the zeolites; however, the presence of some Fe^{2+} (sharp Fe $2p_{3/2}$ peak at 709.9 eV for FeO) cannot be ruled out. A characteristic Fe^{3+} shake-up satellite peak at ~719 eV is observed for both samples further confirming the presence of Fe^{3+}. Analysis of both the Mössbauer and XPS results provide strong support for the assignment of the iron oxide species as maghemite (Fe_2O_3). Fe^{2+} peaks show a shoulder towards lower binding energies than Fe^{3+} peaks. Our peaks did not

show this shoulder, the only species of iron contained being Fe^{3+}, indicating that there is no mixed oxide form.

The N_{1s} XPS are shown in Figure 3.3c, d. The N_{1s} peak at ~401 eV is assigned to an organic amine groups and can be deconvoluted into two components due to amine groups (NH_2) at 399.5 eV and ammonium groups (NH_4^+) at 401.3 eV.[42] Together with the TGA and zeta potential, these results indicate that the amine groups are grafted to the surface of the iron oxide/Y composites. The commercial scale oxide in c showed a very similar pattern to the nano zeolite in d. The binding appears to be similar in both composites.

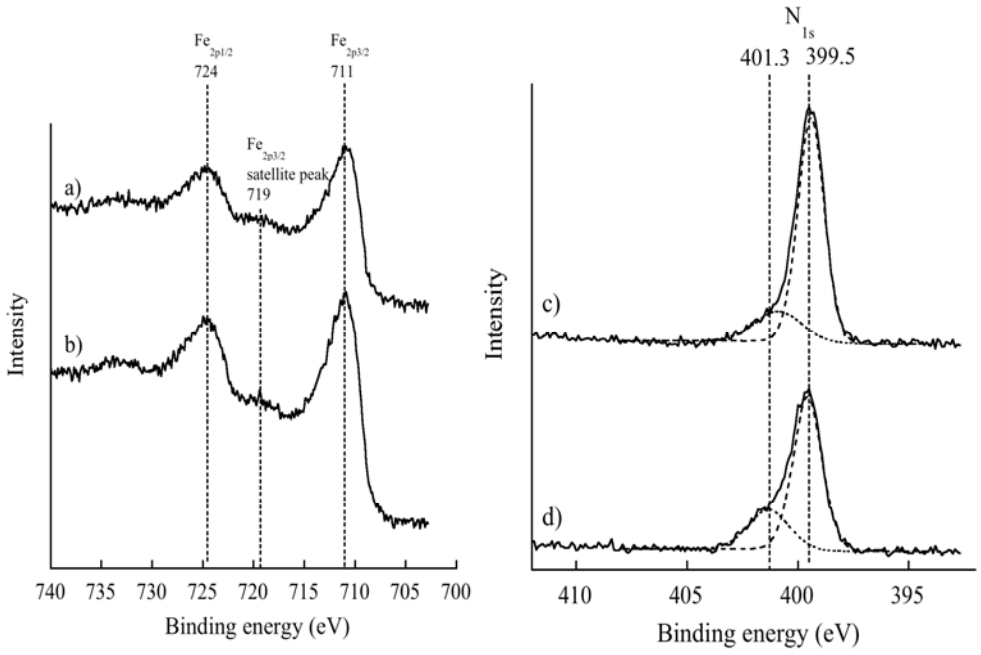

Figure 3.3. XPS spectra of the Fe region of the XPS spectra for a) iron oxide/Y-Zeolyst-APTES and b) iron oxide/Y-nano-APTES. XPS spectra of the N_{1s} region of the XPS spectrum for c) iron oxide/Y-Zeolyst-APTES and d) iron oxide/Y-nano-APTES

Magnetism was a key desired property to facilitate removal of the materials after use. Figure 3.4 shows the magnetism of the particles. This magnetism held in the solution state, the particles were attracted to the magnet and were settled out of solution within 20 minutes. The settling took hours when there was no magnet. The sample in the Figure was commercial zeolite/iron oxide composite, though the property held through in all size ranges.

Figure 3.4. Photograph showing the magnetic properties of the iron oxide/zeolite composites

3.6 Conclusions

Iron oxide zeolite Y composites with surface amine groups and magnetic properties were synthesized. The iron oxide phase in the composite materials was identified as maghemite by Mössbauer and XPS. Crystallinity as well was maintained

during the addition of the iron oxide. While surface area was rather low for these samples, functionalization was comparable to the silicalite crystals. Chromate adsorption for these samples will be addressed in Chapter 4.

CHAPTER 4: CHROMATE ADSORPTION STUDIES

4.1 Introduction

Through surface functionalization, the properties of the nanocrystalline zeolite external surface can be tailored for specific applications [3, 46-48]. For example, the hydrophobicity of the external surface of the zeolite can be increased through functionalization with long chain hydrocarbons, such as octylmethyltrichlorosilane [48]. Similarly, specific functional groups, sulfonic acid groups ($–SO_3H$) or amine groups ($–NH_2$) can be placed on the external surface to promote acid catalyzed reactions or adsorption of DNA, respectively.

Methods used for functionalization of silanol groups in silica based materials, such as mesoporous silica [43, 49-51]can be readily adapted for zeolites with the main difference being that the functionalization occurs exclusively on tzhe external zeolite surface due to the zeolite pore sizes that restrict access to the internal zeolite surface for most organosilane reactants [3, 52]. The advantage of nanocrystalline zeolites in this regard is the extremely high external surface area relative to micron-sized zeolites. High surface area results in a high number of silanol groups, which are primarily found on the surface of the zeolite. These silanol groups are a reactive site, and can be used to attach organic functionalities. The reaction of a surface silanol group on the zeolite external surface with APTES results in an amine-functionalized zeolite as shown schematically in fig 4.1. This method is versatile because many different organosilane reagents can be used to introduce different functionalities to the zeolite surface. These functionalities can

change surface properties in a variety of ways, and can be used for a variety of applications such as adsorption, as seen here.

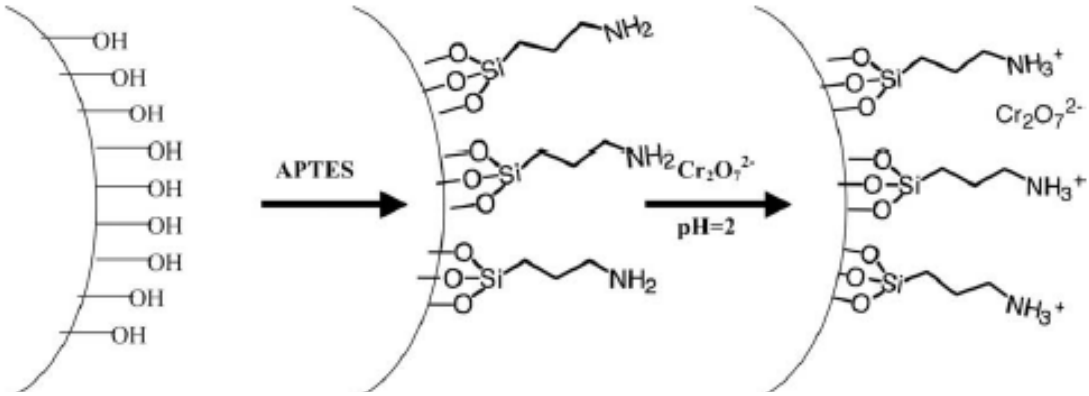

Figure 4.1 Schematic diagram showing the functionalization of silicalite surface with APTES and the protonation of the surface at low pH, followed by the adsorption of chromate

Hexavalent chromium is highly toxic and strictly regulated by the EPA (50 ug/L limit in drinking water) [19, 29, 53]. Hexavalent chromium is found in industrial waste effluents (electroplating, tannery and textile), such that the effluent must be treated before being discharged into the environment to be compliant with EPA regulations. Adsorption is a relatively easy and efficient way to remove hexavalent chromium from waste water effluents and many different adsorbents have been investigated including activated carbon, clays, ion-exchange resins, zeolites and mesoporous silica [1, 13, 20, 28, 40, 54-59]. Recently, there have been several studies of chromate adsorption on amine-functionalized mesoporous silica (MCM-41 and SBA-15) [1, 56-59]and studies of chromate adsorption on organic functionalized natural zeolites [19, 42, 51, 60]. Surface

modification is accomplished through reaction of surface silanol groups with organosilane reagents. This strategy has been widely adopted to functionalize mesoporous silica materials [31, 33, 61]with catalytically active or biologically compatible functional groups [14,33]. SBA-15 and MCM-41 have been functionalized with amine functional groups using organosilanes, such as amino- propyltriethoxysilane (APTES) [20, 32, 55]. The amine functionalized mesoporous silica samples exhibited very high adsorption capacities for chromate.

Silicalite is the purely siliceous form of the zeolite, ZSM-5 which has the MFI structure with 5.6 Å pore diameters. Nanocrystalline silicalite with a crystal size of 32 nm and an external surface area of 100 m^2/g was functionalized with varying amounts of APTES so that the surface properties (such as zeta potential) could be systematically varied and tailored for chromate adsorption. The functionalized silicalite was characterized by powder X-ray diffraction, ^{29}Si magic angle spinning (MAS) NMR, thermal gravimetric analysis (TGA), nitrogen adsorption isotherms, and zeta potential measurements as discussed in Chapter 3. Chromate ($Cr_2O_7^{2-}$) adsorption on the APTES functionalized silicalite (32 nm) and on the iron oxide/zeolite composites was measured in batch experiments.

The iron oxide/zeolite Y composites were effective adsorbents for contaminants, such as Cr^{6+}, Cu^{2+} and Zn^{2+}, from water and were also magnetic, thus facilitating easy removal from aqueous solution using a permanent magnet, as shown in Figure 3.4. Other groups have reported the preparation of magnetic zeolites for seawater purification[41] and biomedical applications[27, 28]. The preparation of magnetic mesoporous silica materials for use as magnetic adsorbents [42] and for biomedical applications[29-31] has

also been reported. Recently, Yeung and coworkers have reported the prepation of a magnetic mesoporous adsorbent with grafted amine groups that is an effective adsorbent for chromium(VI) and arsenic (V). Magnetic iron oxide/zeolite Y composites were also prepared and were then functionalized with amine groups to form a bifunctional, magnetic zeolite. The objective is to prepare a functionalized zeolite material that has enhanced adsorptive properties for chromate due to functional groups on the surface, combined with facile recovery of the adsorbent via the magnetic iron oxide component of the composite material.

In this chapter, the adsorption of chromate on APTES funcionalized silicalite and on magnetic APTES functionalized NaY composites will be discussed. The effect of pH on the adsorption capacity will be investigated. The optimal conditions will be determined for both the iron containing zeolite composites and for functionalized silicalite-1 crystals.

4.2 Experimental Section

Ten milligrams of each zeolite sample was added to 10 mL of 50 ppm solution prepared from $K_2Cr_2O_7$ and controlled at pH 2 with HNO_3. The zeolite/chromate solution was stirred for 2 h at room temperature. After centrifugation, the solids were separated from the supernatant and both were analyzed for chromium content using a Varian 720-ES Inductively Coupled Plasma/Optical Emission Spectrometer (ICP/OES) spectrometer. The chromium concentrations of the solutions were measured directly using the Cr 205.56 nm line of the ICP/OES. The solids were dissolved in 3 mL HF, 1 mL HNO_3 and 15 mL H_3BO_4, diluted to 25 mL with deionized water and the resulting solutions were analyzed for chromium concentration by ICP/OES. Calibrations were done before each

set of measurements using three solutions of known concentration (25, 50 and 100 ppm) made from standards purchased from Inorganic Ventures. Three sample replicates were run for each sample and were averaged to provide the final chromium solution concentrations. Single component adsorption isotherms for $Cr_2O_7^{-2}$were measured using 10 mg of zeolite and 10 mL of solution with concentrations ranging from 0.1 to 2 mM. The samples were allowed to equilibrate for 2 h at room temperature

4.2.1 Chromate Adsorption on Functionalized Silicalite-1

The equilibrium adsorption of chromate (50 ppm) on silicalite-32 nm and APTES functionalized silicalite-32 nm was measured using ICP/OES to determine the chromium concentrations in the solution and in the solids as listed in Table 4.1. The mass balance for the individual experiments ranged from 65% to 100%. The variable mass balance is attributed to the difficulty in recovering all of the solids after the adsorption experiments, leading to lower than predicted amounts of chromium in the solids. Incomplete solid recovery lead to the loss of mass. Very little chromium was adsorbed on the unfunctionalized silicalite despite the fact that it has the highest surface area supporting the idea that the adsorption occurs on the amine functional groups, which are not present on the unfunctionalized silicalite.

The amount of chromium adsorbed on the APTES functionalized silicalite samples increased as the amount of functionalization increased as shown in Table 4.1. The adsorption follows the trend in zeta potential and the reverse of the trend in surface area seen in Chapter 2. An adsorption isotherm for chromate on 0.5 mL APTES silicalite-32 nm is shown in Figure 4.2 and was obtained using chromate concentrations

ranging from 0.1 to 2 mM. The adsorption isotherm was fit using the Langmuir model. The model is described by $q_e = q_{max}*b*C_e/(1+bC_e)$

Table 4.1 Adsorption Properties of Amine Functionalized Silicalite-1

Sample	mmol APTES/g	Zeta potential/ mV	mmol/g Cr adsorbed solution	mmol/g Cr adsorbed solids	Cr/N molar ratio	Mass Balance %
Silicalite-1 0 APTES	0	-41	0	0	N.A.	100
Silicalite-1 .25mL APTES	< .31	-25	0.29	0.28	N.A.	48
Silicalite-1 .5mL APTES	.31	-15	0.43	0.34	1.4	65
Silicalite-1 1mL APTES	.4	-3	0.56	0.42	1.4	81

The monolayer adsorption capacity, q_e is the adsorption capacity in mmol/g, C_e is the equilibrium concentration of chromium in mM, b in mM^{-1} is a constant related to the free energy of adsorption, and q_{max} is monolayer adsorption capacity. The Langmuir fit to the data gave a value of 2.3 mM^{-1} for b and 0.58 mmol/g for $q_{max.}$ Fitting to the Langmuir isotherm assumes that all sites are equal and independent of binding in other sites. The fit is the largest source of uncertainty in these measurements, with an error of generally around 20%.

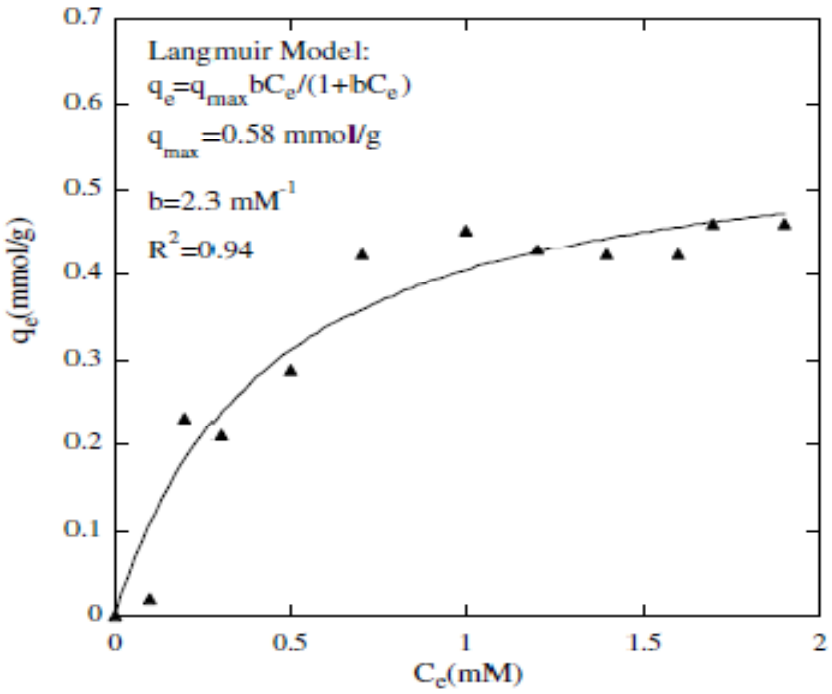

Figure 4.2 Langmuir isotherm fit for Cr on 1 mL amine functionalized silicalite-1

4.2.2 Chromate Adsorption on Iron Oxide/Zeolite Composites

Chromate adsorption on the different zeolite composite samples was evaluated. Initially, the adsorption as a function of pH was investigated for APTES functionalized zeolites and zeolite composites and it was found that acidic pH of ~2 is required for optimal chromate adsorption. The data for the pH dependence of the chromate adsorption is provided in fig 4.3. The acidic pH is required because the amine functional group is protonated at acidic pH values and this is where the chromate anion is believed to electrostatically bind to the zeolite.[12, 24] The amine functionalized zeolite had a higher surface charge at the same pH than the unfunctionalized composites, as seen previously in Chapter 3. The trend in adsorption capacity does not follow the trends in surface areas, since the amine functionalization decreases surface area.

An initial screening of the adsorption on the different zeolite composites was conducted using 40 ppm chromate solution adjusted to pH=2 and the results are listed in Table 4.1. The *iron oxide/Y-Zeolyst* composite showed reduced adsorption capacity relative to the APTES functionalized iron oxide composites *iron oxide/Y-Zeolyst APTES*. The *Y-Zeolyst APTES* showed similar adsorption capacities in this comparison suggesting that the amine functionalization is required for optimal adsorption.

Table 4.2 Adsorption on Iron Oxide/Zeolite Composites in 40 ppm Cr at pH 2

sample	Cr adsorbed/mmol/g	Standard Deviation/ mmol/g
iron oxide/Y-Zeolyst	0.15	0.03
iron oxide/Y-Zeolyst APTES	0.42	0.03
Y-Zeolyst APTES	0.41	0.07
Y Zeolyst	--	--
iron oxide/Y-nano APTES	0.84	0.03
iron oxide/Y-nano	0.6	0.02

Adsorption isotherms (Figure 4.4) were obtained for iron oxide/Y-nano-APTES and iron oxide/Y-Zeolyst-APTES to compare the adsorption in more detail for these two samples. Previous research has shown that adsorption on zeolites can typically be modeled using a Langmuir isotherm. The adsorption isotherms for chromate in Figure 4.4 were obtained using chromate concentrations ranging from 0.1 to 2 mM Cr.

The Langmuir fits to the data are provided in Table 4.3. The adsorption capacities determined from the fit to the Langmuir isotherm are 0.72 and 0.85 mmol/g for iron oxide/Y-nano-APTES and iron oxide/Y-Zeolyst-APTES, respectively. The iron oxide/Y-Zeolyst-APTES sample performs marginally better relative to the iron oxide/Y-nano-APTES sample seen from Table 4.3, though the difference between them is roughly the error in the measurements. This may be due to the slightly higher APTES loading that was achieved on the iron oxide/Y-Zeolyst-APTES sample (see Table 3.4).

To explain these interactions, electrostatic interactions between positively charged amine groups and negatively charged chromate ions are believed to be the basis for adsorption.[12, 22, 24] The chromium adsorption to APTES loading ratios were ~1.5 to 1.2 for the iron oxide/Y-Zeolyst-APTES and iron oxide/Y-nano-APTES samples, respectively, using the adsorption capacity determined from the Langmuir isotherm fitted data. The ratios are similar to the ratio of 1.4 found for two different amounts of functionalization of silicalite-1 reported in Table 4.1. The similarity of ratios could indicate a similar type of binding. The pH effects seen on the iron oxide/Zeolyst-APTES indicate that the adsorption is strongly sensitive to the environment, and probably not strongly bonded-changing the pH caused the dichromate to desorb with a change in pH. The equilibria discussed in chapter 2 indicate the effect on protonation and zeta potential.

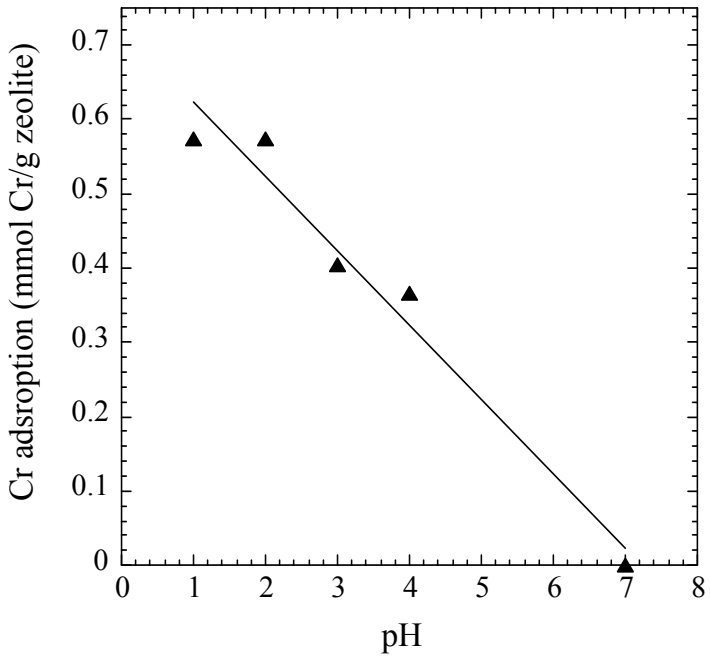

Figure 4.3. Chromate adsorption on iron oxide/Y-Zeolyst-APTES as a function of pH. The pH was adjusted by HNO_3 and NaOH. 10 mL of 40 ppm chromate solution was used.

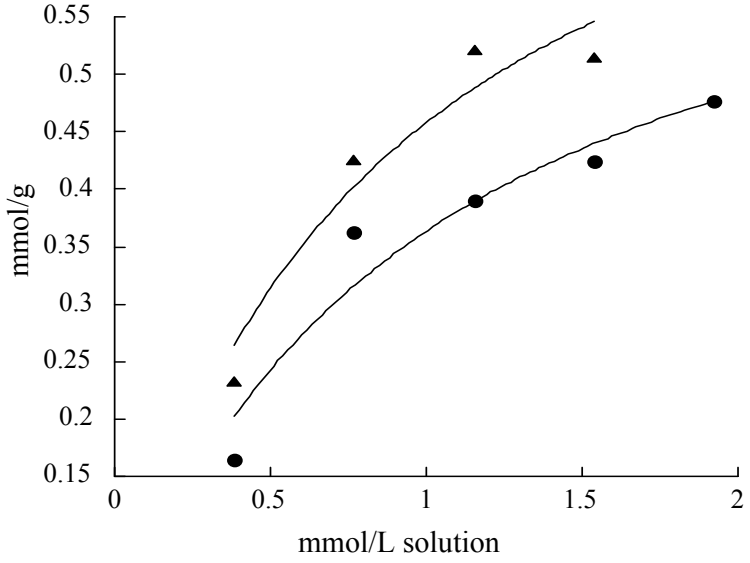

Figure 4.4. Chromate adsorption at pH 2 on iron oxide/Y-Zeolyst-APTES (triangles) and iron oxide/Y-nano-APTES (circles) fit to a Langmuir isotherm.

Functionalization of both iron oxide/Y-Zeolyst-APTES and iron oxide/Y-nano-APTES composites increases the chromium adsorption from 0.14 to 0.42 mmol/g at 40 ppm. Both the iron-containing functionalized samples were just as effective as the Y-Zeolyst-APTES samples without iron for chromate adsorption. The surface area loss due to the iron doesn't appear to affect the adsorption capacity of the materials, suggesting that the adsorption occurs exclusively on the external surface. The difference in surface areas can be seen in Table 4.1, while no difference in adsorption is noticed.

Table 4.3: Langmuir Adsorption Isotherm Parameters [a]

Sample	b (mM^{-1})	q_{max} (mmol/g)	R
iron oxide/Y-nano_APTES	1.0 (0.4)	0.72 (0.13)	0.964
iron oxide/Y-Zeolyst-APTES	1.2 (0.6)	0.85 (0.18)	0.966

[a] Fitting errors are given in parenthesis, as the fitting is the most significant source of error.

The iron oxide phase does not interfere with the surface interactions between chromate and the amine functional groups on the surface. The requirement of such low pH values may be an impediment to practical applications of this technology. Applications would be more likely to be mining or industrial uses, before water is returned to the environment. Recent results suggest that improved chromate adsorption can be obtained at higher pH by preadsorbing Fe^{3+} to the amine functionalized

material.[6, 21, 22, 44] The composite powder material is attracted to the wall of the vial by the magnetic field. This suggests that these materials will be easily removed from aqueous solution after use with a permanent magnet.

4.3 Results and Discussion-Comparison of Adsorption Capacities

The highest adsorption capacity for $Cr_2O_7^{2-}$ on silicalite-1 obtained in this study was approximately 0.54 mmol/g silicalite-32 nm for the silicalite sample containing the highest concentration of amine groups (silicalite-1 32 nm 1mL) as seen in Table 4.1. While this adsorption capacity is comparable to chitosan (0.65 mmol/g) [62, 63] and much greater than organo-modified zeolite (0.0041 mmol/g) [13], it is 2–3 times lower than the adsorption capacities achieved for functionalized mesoporous materials, such as amine modified MCM-41 and amine-modified SBA-15[12, 13, 15, 18, 34, 56]. The larger adsorption capacity for mesoporous silica materials is attributed to the higher surface area and higher concentrations of functional groups that can be achieved in mesoporous materials. Table 4.4 shows a comparison of various chromate adsorption capacities.

However, the Cr/N molar ratio obtained in this study is greater than one (Table 4.1) suggesting that all of the functional groups are accessible to the chromate. This is in contrast to mesoporous materials where overall adsorption capacity per gram of solid is higher but the Cr/N ratio is lower varying from 0.5 in ref [21] to 0.8 in ref [30] in different studies. Since some degradation of zeolite structure is observed by X-ray diffraction, future work will also focus on using milder conditions for the adsorption process so that the zeolite framework will remain stable.

The approximately 1:1 correspondence between surface amine group concentration and Cr adsorption suggests that the interaction is electrostatic and that all

of the functional groups are accessible to the chromate. Potentially, the adsorption capacity for nanocrystalline silicalite could be increased by increasing the external surface area and the concomitantly increasing the functionalization of the external surface.

The external surface area for silicalite (assuming a cubic crystal) is given by SA_{ext} = 3214/x where x is the crystal size in nanometers [64]. Decreasing the crystal size by a factor of two should double the external surface area. For a 30 nm silicalite crystal, the external surface area is 100 m^2/g and the external surface area for a 15 nm silicalite crystal is 200 m^2/g. Therefore, we would predict that an approximately 2-fold increase in adsorption capacity for chromate anions could potentially be gained by going to smaller silicalite crystal sizes. Extremely small crystals are unstable. However, silicalite-1 crystals with an MFI structure are believed to be stable at these sizes

Table 4.4 Comparison of Zeolite Adsorption Capacities in mg/g

	amine MCM	amine zeolite	unfunc zeolite	tannin	clay	Chitosan
literature	23	3.95	2.4	1.6	55	27
This work (silicalite)	27	23.9	1.84			
ref	[50]	[18]	[18]	[59]	[59]	[59]

The iron oxide had a maximum adsorption capacity slightly higher than the silicalite-1 crystals, despite lower surface areas. This is believed to be related to the larger number of functional groups on these materials. Tubes all showed lower adsorption than the single crystals, no matter where they were functionalized. The difference in iron oxide

composite adsorption capacity was not large enough that it changes the comparison to literature adsorbents discussed earlier.

Chromate speciation and pH dependence is an important part of the adsorption picture[65, 66] At pH 2, chromate is mostly in the form of hydrogen chromate $Cr_2O_7^{-2}$. The speciation diagram is found in Figure 4.5. This form of chromium appears to be more easily adsorbed than the chromate or hydrogen chromate found at higher pH or lower pHs, as shown by the adsorption on the magnetic composite. Dichromate would help explain the greater than 1:1 ratio of Cr:N seen on the silicalite-1 and iron samples.

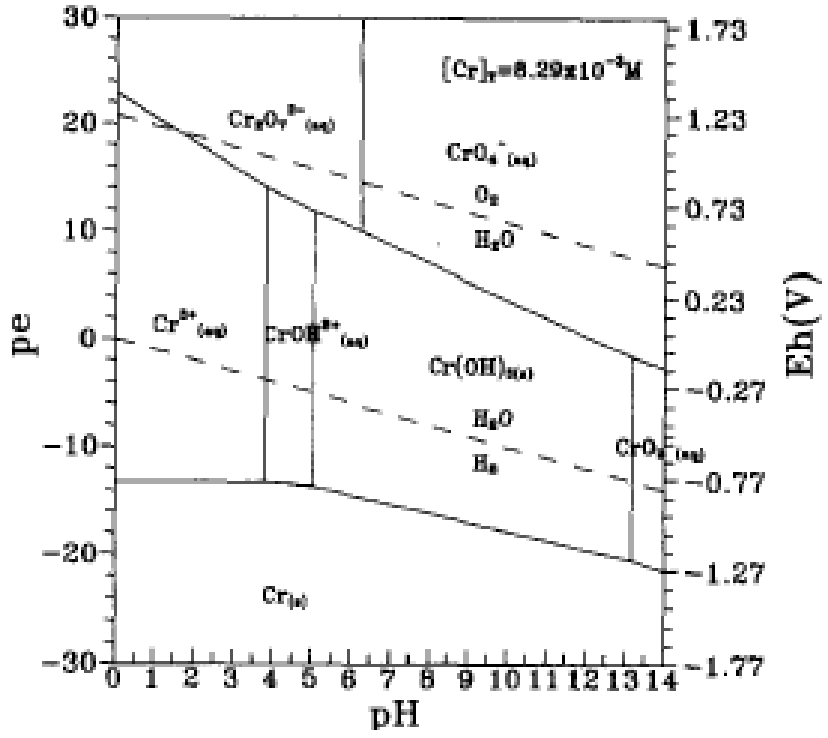

Figure 4.5 Diagram showing chromate speciation as a function of pH

The pH effects on adsorption show a clear negative trend, as seen in Figure 4.3. Going up to pH 7 halts all adsorption. The effect can be used as a method for desorption and recycling method.

4.4 Conclusions

Chromate was adsorbed on both silicalite-1 nanocrystals and Fe_2O_3/zeolite composite. The surface area after functionalization decreases, but this did not appear to adversely affect the chromate adsorption, suggesting that adsorption occurs on the external surface. Adsorption is dependent on the loading of functional group and the surface charge, consistent with an electrostatic interaction. The maintenance of adsorption capacity coupled with the easy removal render these magnetic zeolite composites an attractive material for large scale water purification applications.

Crystallinity as well as adsorption capacity was maintained under adsorption conditions. One potential drawback of this method is the low pH's required for optimal adsorption capacity. Methods of adsorbing cations to the amine functional group to increase the optimal pH for adsorption have been suggested for the future work.

Nanocrystalline silicalite-1 with a crystal size of 32 nm was functionalized with varying amounts of APTES. Adsorption capacity increased as the amount of APTES functionalization increased. The maximum adsorption capacity was approximately 0.6 mmol Cr/g zeolite. These results demonstrate that the external zeolite surface of nanocrystalline zeolites can be tailored through functionalization in order to increase the adsorption capacity for a specific adsorbate, in this case chromate. Future improvements in adsorption capacity of nanocrystalline zeolites can potentially be achieved by further decreasing the zeolite crystal size and thus increasing the external surface area.

CHAPTER 5: ARSENIC ADSORPTION ON IRON CONTAINING ZEOLITE COMPOSITES.

5.1 Introduction

Arsenic in drinking water is a global problem. Arsenic occurs naturally in rocks and soil, water, air, and plants and animals. It can be further released into the environment through natural activities such as volcanic action, erosion of rocks and forest fires, or through human actions. Approximately 90 percent of industrial arsenic in the U.S. is currently used as a wood preservative, but arsenic is also used in paints, dyes, metals, drugs, soaps and semi-conductors. High arsenic levels can also come from certain fertilizers and animal feeding operations. Industry practices such as copper smelting, mining and coal burning also contribute to arsenic in our environment.

Arsenic is a large problem in groundwater in Bangladesh and other places in the world. The current recommended exposure level by the World Health Organization (WHO) and the legal limit in the US is 10 ppb.[22] The ideal level for health is believed to be even lower than this value, however measuring much lower concentrations can be difficult at best, and 10 ppb is the provisional limit. Many natural sources in the US and other parts of the world give levels of above 50 ppb. Arsenic exposure can cause a variety of mental and physical symptoms, including cancer, neurological problems and death.

Adsorption has been shown to be an effective method for arsenic removal. Zeolites have been shown to be useful as adsorbents because of their high surface area.[20, 67-71] Surface modification has been shown to be applicable in the case of mesoporous materials, and has been shown to be useful in zeolites as well.[1, 16, 72-77].

To expand the pH range to neutral pH, previous studies have shown that Fe^{3+} preadsorbed on amine functionalized materials facilitates anion adsorption at neutral pH. This research aims to take advantage of these interactions and previously seen adsorption behavior of anions on zeolite[43] to facilitate removal of arsenate species from water solutions at neutral pH. Iron-exchanged zeolite Y, iron oxide/zeolite Y, iron oxide/Y-APTES and iron oxide/Y-APTES –Fe^{3+} composite materials were prepared as and were evaluated for arsenic removal from aqueous solution.

5.2 Materials Synthesis

5.2.1 Synthesis of Iron Oxide/Zeolite Composites

Nanocrystalline NaY (Y-nano) with a size of approximately 58 nm and Si/Al=1.9 was synthesized according to a previously published procedure[64]. Textural properties of NaY (Zeolyst and Y-nano) are provided in Table 5.1. Following the procedure of Oliveira and co-workers[39], iron oxide/Y composites were formed. NaY (Zeolyst or nano) was added to 200 mL of nitrogen purged water and then 30 mL of a 1:2 mol ratio of $FeCl_3$:$FeCl_2$ was added dropwise in a glove bag under nitrogen. The resulting iron oxide/zeolite composite will be designated *iron oxide/Y-Zeolyst* or *iron oxide /Y-nano*. The composite materials were washed with water and ethanol, dried in an oven overnight at 368 K, and then annealed under N_2 for 6 h. at 723K.

5.2.2 APTES Functionalization of Zeolite Composites

After annealing, the iron oxide/zeolite material was functionalized with aminopropyltriethoxysilane (APTES) according to literature procedures.[43] 0.5 g of iron oxide/zeolite composite (or zeolite Y) was refluxed in 50 mL toluene and 1.5 mL

APTES for 4.5 h. The samples were washed with water and ethanol and dried at room temperature. These APTES functionalized samples are designated as *iron oxide/Y-nano-APTES and iron oxide/Y-Zeolyst-APTES.*

5.2.3 Fe^{3+} exchanged iron oxide/Y-APTES

Following literature procedure[42] iron oxide/Y-APTES and Y-nano were ion exchanged overnight from 1M ethanol solution of $FeCl_3$ (Aldrich). Samples were then washed with ethanol and dried at room temperature. These exchanged samples are designated *iron oxide/Y-nano-APTES-Fe^{3+}, iron oxide/Y-Zeolyst-APTES-Fe^{3+}* and *iron-exchanged Y-nano.*

5.2.4 Characterization

The zeolite Y and zeolite Y composite samples were characterized by powder X-ray diffraction (XRD), nitrogen adsorption isotherms (BET method), inductively coupled plasma optical emission spectroscopy (ICP-OES), zeta potential measurements, thermal gravimetric analysis (TGA), Mössbauer spectroscopy and X-ray photoelectron spectroscopy (XPS).

XRD patterns were obtained using a Rigaku Mini Flex II system with a Cobalt X-ray source and a Fe K-beta filter to filter out the K-beta lines from the Co source. XRD patterns were collected between $2\theta = 5$ and 75 degrees with a step size of 0.04° and were analyzed with MDI Jade software. Nitrogen adsorption isotherms were obtained on a Quantachrome Nova 4200e multipoint BET apparatus using approximately 0.1 g of sample for each measurement. Prior to the N_2 adsorption, each sample was vacuum degassed at 120 °C for 2–3 h. The specific surface area was calculated by the BET method using the Nova 4200e instrument software.

ICP/OES analysis was conducted using a Varian 720-ES ICP/OES spectrometer. Typically, 10 mg of the sample was digested in 1.6 mL 70:30 HCl: HF mixture. Then 0.56 mL of concentrated nitric acid and 8.4 mL of 5% boric acid were added and the volume was adjusted to 14 mL with deionized water. 1 ppm solution of yttrium was used as an internal standard during the measurements. TGA was performed on a TA Instruments Q500 TGA by heating from room temperature at 5.00 °C/min to 1000 °C under N_2. The results were analyzed using TA Universal Analysis with the amine peak appearing at approximately 350 °C.

The iron oxide species were characterized using Mössbauer spectroscopy and XPS. Mössbauer spectra were collected in transmission mode with a constant acceleration drive system and a ^{57}Co source. Samples for Mössbauer spectroscopy were mounted in a top loading Janis exchange-gas cryostat. The source was maintained at room temperature during analysis. Data were calibrated against an α-Fe metal foil collected at room temperature. Spectral fitting was done with the Recoil software package. The Mössbauer spectra were compared to known spectra of superparamagnetic iron oxide materials. For XPS spectroscopy, a monochromatic Al K_α X-ray source was used to scan the samples. The pressure in the analysis chamber was maintained in the range of $1.33*10^{-6}$ to $1.33*10^{-7}$ Pa. Low energy electrons were used to maintain a uniform charge on the samples. Wide energy range survey scans were acquired using following parameters: energy range from 1200 to -5 eV, pass energy of 160 eV, step size of 1 eV, dwell time 200 ms, x-ray spot size 700 x 300 mm. High resolution spectra were acquired using following parameters: energy range of 50 - 20 eV depending on the peak examined, pass energy of 20 eV, step size of 0.1 eV, dwell time of 1000 ms. Three

sweeps were used for the Fe 2p region to enhance signal to noise. The spectra were fit using Shirley background Gaussian-Lorentzian (30) fitting program with the Kratos software package

5.2.5 Arsenate Adsorption Experiments

10 mg of each iron oxide/zeolite Y composite sample was added to 10 mL of solution of the given concentration prepared from $KHAsO_4$ from Aldrich. The pH was adjusted to 2 with nitric acid for low pH samples and left unmodified at pH~7 for higher pH samples. The mixture was stirred overnight at room temperature. After centrifugation, the solids were separated from the supernatant and analyzed for arsenic content using ICP/OES (Varian 720-ES). The arsenic concentrations of the solutions were measured directly using the As 188.6 nm line. Calibrations were done before each set of measurements using three solutions of known concentration (25, 50 and 75 ppm) made from standards purchased from Inorganic Ventures. Three sample replicates were run for each sample and were averaged to provide the final arsenic solution concentrations.

5.3 Results and Discussion

5.3.1 Physicochemical Characterization of Iron Oxide/zeolite Y Composites

Powder XRD was used to evaluate crystallinity and potentially identify the different component phases of the iron oxide/zeolite materials. The powder XRD patterns of as-synthesized iron oxide [39], zeolite Y-Zeolyst and iron oxide/Y composites are shown in Figure 5.1. The XRD powder pattern for the parent Y zeolite without modification is shown in Figure 5.1a for comparison with the composite materials. The XRD powder patterns of the iron oxide/Y-nano-APTES, iron oxide/Y-

nano-APTES-Fe^{3+}, and iron oxide/Y-commercial-APTES-Fe^{3+}, are shown in Figure 5.1 b, c and d, respectively. The XRD pattern of maghemite is shown for comparison. The dominant features are the zeolite Y reflections with possible weak contributions from the iron oxide phase at a $2\theta \sim 42°$. The XRD lines of the iron oxide/Y-nano-APTES-Fe^{3}

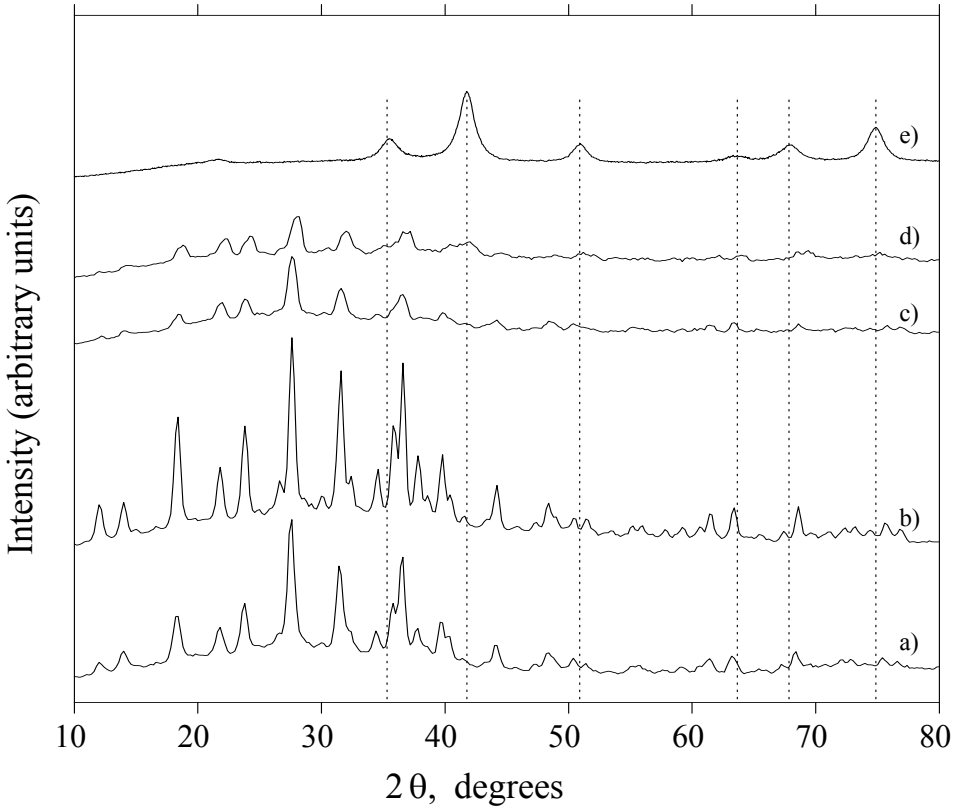

Figure 5.1 Powder X-ray diffraction patterns for a) Y-nano, b) iron oxide/Y-nano-APTES, c) iron oxide/Y-nano-APTES-Fe^{3+} and d) iron oxide/Y-commercial-APTES-Fe^{3+} and e) iron oxide (Fe_2O_3) as synthesized. Dashed lines indicate the iron oxide (Fe_2O_3 and/or Fe_3O_4) reflections.

The specific surface areas of the samples were measured by nitrogen adsorption $^{+}$ composite (Figure 5.1c) and iron oxide/Y-commercial-Fe^{3+} composite (Figure 5.1d) are

significantly broadened relative to the nano Y (Figure 5.1a). There appears to be some loss of crystallinity that is causing the decrease in powder XRD intensity. The line broadening could also be attributed to a decrease in particle size.

Zeta potential and BET analysis and are listed in Table 5.1. The external surface area for as-synthesized Y-nano was measured with the template still in the pores of zeolite Y and was 70 m^2/g which can be used to calculate the particle size assuming cubic crystals. The external surface area corresponds to a NaY crystal size of approximately 58 nm according to $x=4061/S_{ext}$ where x= crystal size in nm and S_{ext} is the external surface area.[78] The iron oxide/Y (both nano and Zeolyst) composites exhibited a decrease in specific surface area after functionalization or iron loading (Table 5.1). In both cases, the surface areas of iron oxide/Y-nano- APTES-Fe^{3+} and iron oxide/Y-Zeolyst- APTES-Fe^{3+} were 33 and 17 m^2/g, respectively. The decrease of surface area is due to blocking of the zeolite pores by the iron oxide species and/or functional groups and has been observed previously for related materials. Pore blocking leads to restricted access to the internal zeolite surface.

The BET surface areas for the iron oxide/Y-Zeolyst-APTES $Fe^{3+}$and iron oxide/Y-nano-APTES Fe^{3+} were extremely small 33 and 16 m^2/g, respectively. The surface areas are decreased by blocking increasingly in each step of the synthesis, as seen from Table 5.1. Fe^{3+} exchange did not decrease the zeta potential back down to the range for magnetic composites before functionalization. The positive surface charge from the protonated amines remains.

The zeta potential varies with pH and ionic strength and represents the surface charge. [36] The zeta potential for the Zeolyst Y and nano-Y and the iron oxide / zeolite

composites at pH=7 are listed in Table 5.1. The zeta potential of the parent Y zeolites reflects the protonation of surface hydroxyl group. The zeta potentials (@pH=7) were -18 and -15 mV, for the Zeolyst and nano NaY samples, respectively. The zeta potential increased slightly after exchange with iron and functionalization with APTES. When zeolite Y is functionalized with APTES, the zeta potential will change relative to the parent zeolite due to the protonation of the surface amine groups as shown in Chapter 2 Functionalization of zeolite Y with APTES leads to an pH-dependent increase in the zeta potential relative to the parent zeolite. Similarly, APTES functionalization of iron oxide/Y composites leads to a similar increase in zeta potential.

Table 5.1 Physicochemical Properties of Iron Containing Zeolite Composites

sample	Zeta potential[a]/ mV	Surface.Area[b] m^2/g
HY nano	-15	550
iron oxide /Y-nano	-11	88
iron oxide/Y-nano-APTES	-8	58
iron oxide/Y-nano-APTES-Fe^{3+}	-5.4	33
HY Zeolyst	-18	440
iron oxide/Y-Zeolyst	-15	420
iron oxide/Y-Zeolyst-APTES	-7	160
iron oxide/Y-Zeolyst-APTES-Fe^{3+}	-6	16.
Fe exchanged	-12	73.

[a]Zeta potential was measured at pH=7

[b] estimated %error for the surface area measurement is 8%

5.3.2 Characterization of Iron by Mossbauer Spectroscopy and XPS

Mossbauer spectra of iron oxide/Y-Zeolyst-APTES-Fe^{3+}, iron oxide/Y-nano-APTES-Fe^{3+} and iron-exchanged Y-nano are shown in Figure 5.2 a-c. The signal to noise is poor and precludes spectral fitting. The spectra are complex with magnetic and paramagnetic iron species present in the samples. There appear to be multiple forms of iron present but due to the poor signal to noise, the spectra cannot be deconvoluted. Samples showed some sorbed Fe^{3+} in addition to the ordered phase, as evidenced by the

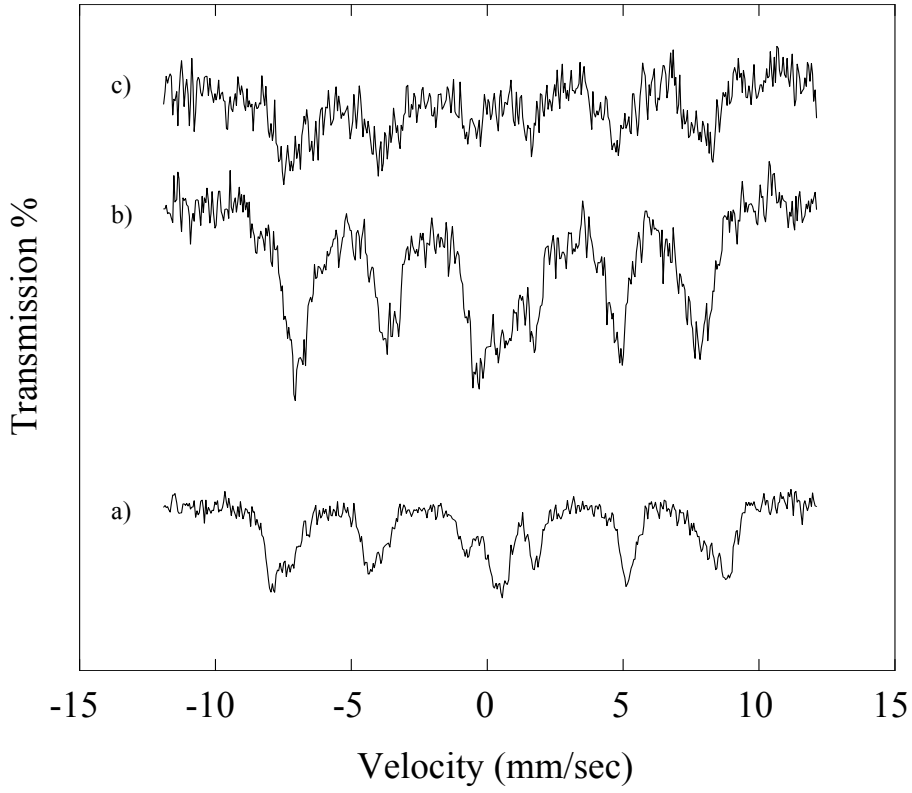

Figure 5.2 Mössbauer spectra of iron containing zeolite composites.
Mössbauer spectra obtained at 13 K for a) iron oxide/Y-Zeolyst-APTES-Fe^{3+}, b) iron oxide/Y-nano-APTES-Fe^{3+} and c) iron oxide/Y-nano

presence of two different Fe^{3+} sextets in the spectra at 13K. The multiple phases and weak signals makes it difficult to interpret the spectra in more detail.

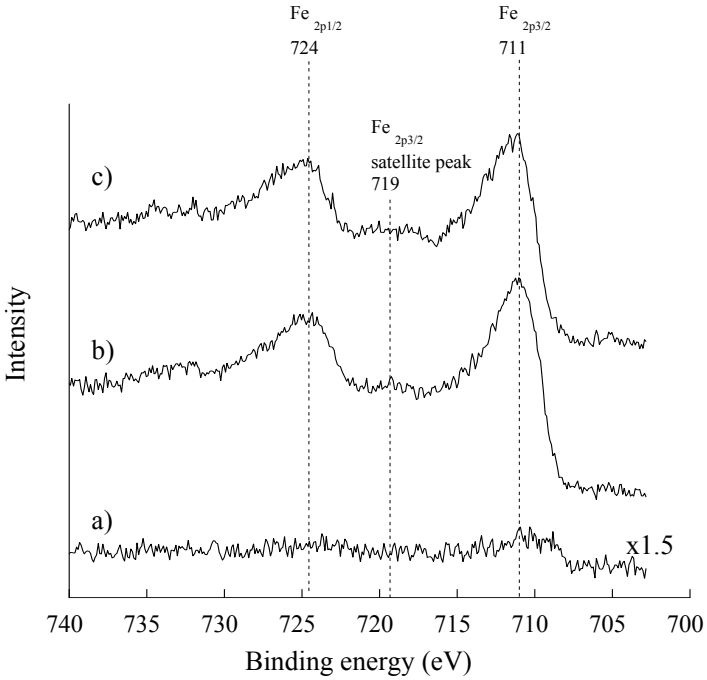

Figure 5.3: XPS spectra of the Fe region of the XPS spectra for a) iron oxide/Y-nano-APTES-Fe^{3+} and b)Iron-exchanged Y-nano and c) iron oxide/Y-Zeolyst

XPS spectra of iron oxide/Y-nano-APTES-Fe^{3+}, iron-exchanged Y-nano and iron oxide/Y-Zeolyst obtained in the Fe 2p region are shown in Figure 5.3a,b,c respectively. The Fe 2p region of the XPS spectrum is complex and often includes contributions from overlapping peaks of Fe^0, Fe^{2+} and Fe^{3+} oxides. Fe_2O_3 (Fe^{3+}) has a binding energy of 711.1 eV (with shake-up satellite peak at 719.8 eV[44]) and FeO (Fe^{2+}) has a binding energy of 709.9 eV (with shake-up satellite peak at ~715 eV[44]). The mixed valence compound Fe_3O_4 has a binding energy ranging from 710.5 to 711.2 eV.[45] These iron

oxide species have been previously observed in XPS studies of iron-exchanged zeolites[43-45] A sharp Fe $2p_{3/2}$ peak is seen at a binding energy of ~711 eV in Figure 5.3 b,c. This peak is primarily attributed to Fe^{3+} oxide species present in the zeolites; however, the presence of some Fe^{2+} (sharp Fe $2p_{3/2}$ peak at 709.9 eV for FeO) cannot be ruled out. A characteristic Fe^{3+} shake-up satellite peak at ~719 eV is observed for both samples (Figure 5.3 b,c) further confirming the presence of Fe^{3+}. The XPS spectrum in Figure 5.3a is very weak and difficult to interpret.

5.3.3 Arsenic Adsorption on Iron-Containing Zeolite Materials

Arsenic typically adsorbs and reduces on most iron containing species[79]. Total equilibrium measurements performed reflect loss from both of these mechanisms. The equilibrium removal of arsenic on the iron-containing zeolites at pH=7 and pH=2 are listed in Table 5.2. The samples containing Fe^{3+} showed the greatest removal at pH 7 relative to pH 2. The data in the table shows some removal on Y-nano-APTES, Iron oxide/Y-nano-APTES, Iron oxide/Y-nano-APTES-Fe^{3+}, and Iron oxide/Y-Zeolyst-APTES-Fe^{3+}. The greatest adsorption capacities of approximately 0.6 mmol/g was observed for iron oxide/Y-Zeolyst-APTES-Fe^{3+} and iron-exchanged Y-nano at pH 7, however.

Previous research has shown that adsorption on zeolites can typically be modeled using a Langmuir isotherm. The adsorption isotherm for arsenate adsorption on iron-exchanged Y-nano is shown in Figure 5.3. The adsorption isotherm was fit using the Langmuir model where q_e is the adsorption capacity in mmol/g, C_e is the equilibrium concentration of arsenic in mM, b is a constant related to the free energy of adsorption,

and q_{max} is monolayer adsorption capacity. [16] The fitted parameters are b=3.0 (8) and q_{max}=0.57 (4) mmol/g.

Table 5.2 Adsorption on Iron Containing Zeolite Composites

Sample	As adsorption (mmol/g)	
	@pH=2	@pH=7
Y-nano	---	0.02
Y-nano-APTES	0.15	0.12
Iron oxide /Y-nano	0.11	0.09
Iron oxide/Y-nano-APTES	0.13	0.02
Iron oxide/Y-nano-APTES-Fe^{3+}	0.20	0.45
Iron oxide/Y-Zeolyst-APTES-Fe^{3+}	0.18	0.65
Iron-exchanged Y-nano	--	0.60

Table 5.3 Comparison of Iron Containing Materials for As Adsoprtion

Material	Adsorption(mmol/g)	Chuita[65]
synthetic zeolite	0.96	Mayo[69]
maghemite	0.55	Yokoi[50]
Fe^{3+}-MCM-41	1.5	Menhaje-Bena[72]
Fe modified natural zeolite	0.6	Kumar[66]
amino MCM-41	0.24	Payne[70]
activated carbon	0.5	Davila-Jimenez[71]
Fe clilntopolite Tuff	0.1	Chuita[65]

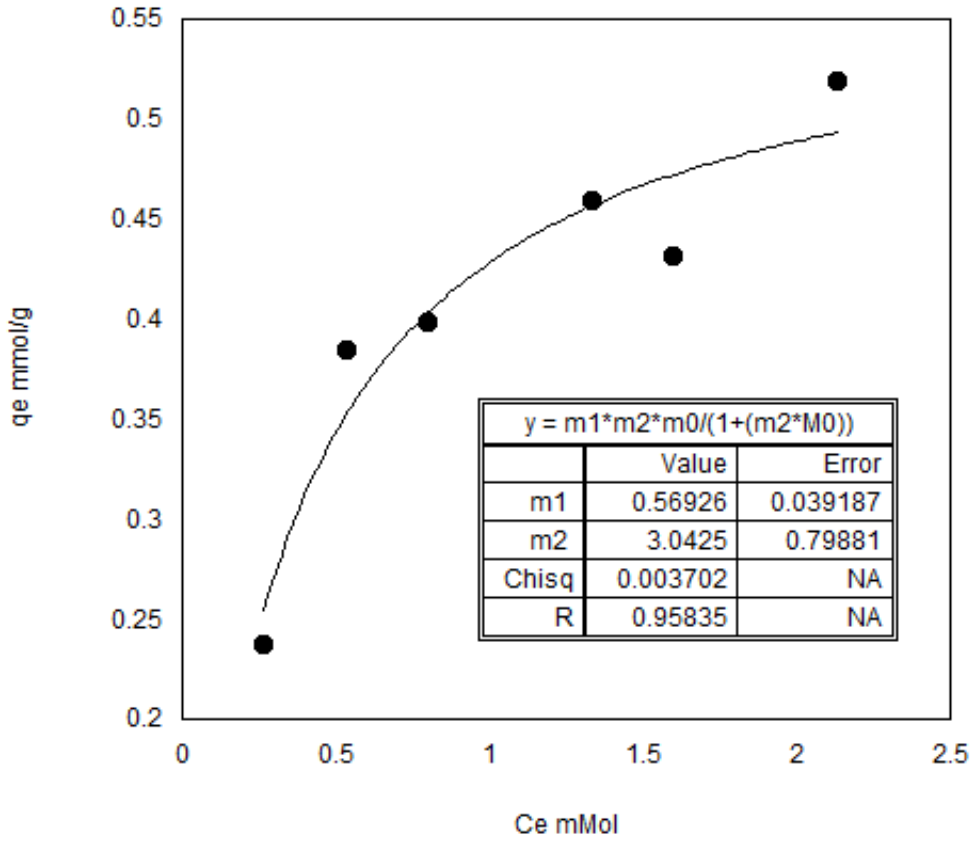

Figure 5.4 Langmuir isotherm fit for Fe^{3+} exchanged zeolite

For comparison, the arsenic adsorption capacities for related adsorbents are provided in Table 5.3. The adsorption capacities of activated carbon (0.5 mmol/g) and maghemite (0.55 mmol.g) are similar to those reported here for the zeolite composites. Fe^{3+}-MCM-41 has a higher arsenic adsorption capacity of 1.5 mmol/g most likely due to the increased surface area of these materials relative to the zeolites used in this study.

The arsenate interaction with surface Fe^{3+} is expected to be electrostatic. However, it is known that iron arsenate interactions can be quite complex. The adsorbed or exchanged Fe^{3+} is required for adsorption at pH 7.

The %composition of the zeolite samples measured by ICP/OES is listed in Table 5.4. The last column of Table 5.4 shows the amount of sorbed Fe calculated by difference using the iron % composition before and after iron adsorption. Similar amounts of Fe^{3+} are sorbed on the Iron oxide/Y-Zeolyst-APTES-Fe^{3+} and iron-exchanged Y-nano. They both show very similar adsorption capacities for Fe^{3+}. Some of the iron was leached into solution; however, the magnetic properties of the material remained unchanged. Iron leaching was lower for the iron oxide/Y-APTES samples relative to iron-exchanged Y-nano with values of ~30-35 mg $g^{-1*}L^{-1}$ and ~ 200 mg $g^{-1*}L^{-1}$, respectively. The magnetic properties of the iron oxide/Y composites can be observed visually. The composite powder material is attracted to the wall of the glass vial by applying a magnetic field with a permanent magnet. This suggests that these materials will be easily removed from aqueous solution using an inexpensive permanent magnet. This makes the magnetic composites much simpler and more convenient to use relative to some other adsorbents. The Fe-exchanged samples do not share this magnetic property, a

possible drawback for commercial applications, because these samples required centrifugation for separation.

Table 5.4 Elemental Compositions (wt %) of Iron-Containing Zeolites Measured by ICP/OES

Sample	**Si**	**Al**	**Fe**	**Fe ads**
Commercial NH_3-/Fe_2O_3 -Fe^{3+}	11.5%	5.0%	10.5%	.009 mmol/g
nano NH3-/Fe_2O_3 -Fe^{3+}	10.5%	6.5%	6.8%	.001 mmol/g
Commercial Fe_2O_3 Y	11.9%	6.2%	5.5%	0
nano Fe_2O_3 Y	29.7%	16.0%	4.9%	0
Fe^{3+} exchanged Y	11,5%	8.5%	5.2%	.0095 mmol/g

Some of the iron was desorbed into solution; however the magnetic properties of the material remained unchanged. Iron leaching was lower for the magnetic/amine/Fe^{3+} samples 30-35 $mg^{*}g^{-1*}L^{-1}$ as compared to the Fe^{3+} exchanged samples of approximately 200 $mg^{*}g^{-1*}L^{-1}$. The magnetic properties of the iron oxide/Y composites can be observed visually. The composite powder material is attracted to the wall of the vial by the magnetic field. This suggests that these materials will be easily removed from aqueous solution after use with a permanent magnet. This makes the magnetic composites much simpler and more convenient to use than many materials. The Fe exchanged samples do

not share this magnetic property, a possible drawback for commercial applications, because these samples required centrifugation.

The form of As that are removed is an area of interest. All As in these experiments started out as As(V) and is believed to remain that way due to atmospheric oxygen, which has a pE(a measure of oxidation potential) of around 8. No samples were kept in an anoxic environment. From Figure 5.5, taken from ref[80, 81] the main form of As will depend on pH but will be some form of arsenate.

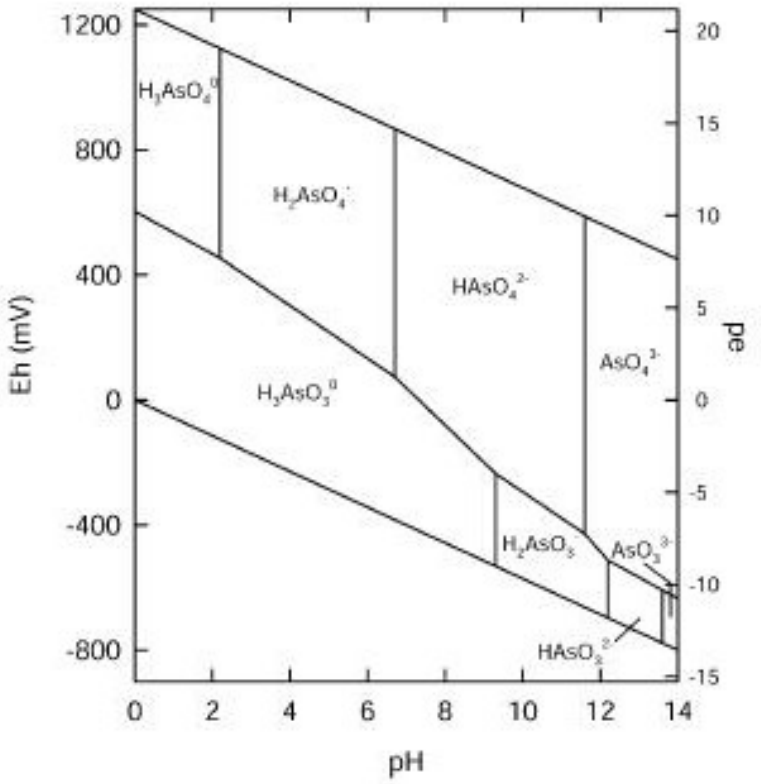

Figure 5.5 Pourbaix diagram of arsenic species

5.4 Conclusions

The magnetic zeolite composites with adsorbed iron and the iron-exchanged zeolite show both easy removal and sufficient adsorption of arsenate from aqueous

solution for environmental applications. The iron oxide phase in the composite materials was investigated by Mossbauer and XPS but weak signals precluded definitive assignments. The surface area after functionalization is small, but this did not appear to adversely affect the adsorption. Adsorption is dependent on the loading of Fe^{3+}. The maintenance of adsorption capacity coupled with the easy removal renders these magnetic zeolite composites an attractive material for large scale water purification applications. Crystallinity as well as adsorption capacity was maintained somewhat under adsorption conditions. The optimal pH range was found to be near neutral-pH 7.

CHAPTER 6: CONCLUSIONS AND FUTURE WORK

Nanocrystalline silicalite and hollow silicalite tubes were functionalized with organosilanes and iron oxide zeolite Y composites with surface amine groups and magnetic properties were synthesized. Nanocrystalline silicalite with a size of approximately 30 nm was systematically functionalized with varying amounts of APTES. The APTES functionalized silicalite was characterized by powder XRD, solid state ^{29}Si MAS NMR, TGA, and zeta potential. The trend of decreasing surface area and zeta potential with increasing APTES functionalization was observed. These results demonstrate that the external surface of nanocrystalline zeolites can be tailored through functionalization in order to achieve desired results. Hollow silicalite tubes were functionalized with APTES or MPTMS. ^{29}Si MAS NMR and XPS were used to characterize the resulting sulfur functional groups. Nanocrystalline silicalite with a crystal size of 32 nm was functionalized with varying amounts of APTES and chromate adsorption was measured. Adsorption capacity increased as the amount of APTES functionalization increased. The maximum adsorption capacity was approximately 0.6 mmol Cr/g zeolite for silicalite-1. These results demonstrate that the external zeolite surface of nanocrystalline zeolites can be tailored through functionalization in order to increase the adsorption capacity for a specific adsorbate, in this case chromate.

For iron oxide composites, the iron oxide phase in the composite materials was identified as maghemite by Mössbauer and XPS. Crystallinity of the zeolite was maintained during the addition of the iron oxide. While surface area was rather low for

these samples, functionalization was comparable to the silicalite crystals. Iron oxide composites were tested for adsorption of chromate and arsenate anions

The magnetic zeolite composites with adsorbed iron and the iron exchange zeolite show both easy removal and sufficient adsorption of arsenate from aqueous solution for environmental applications. The iron oxide phase in the composite materials was identified as mixed by Mössbauer and XPS. The surface area after functionalization is small, but this did not appear to adversely affect the adsorption. Adsorption is dependent on the loading of iron $^{3+}$. The maintenance of adsorption capacity coupled with the easy removal renders these magnetic zeolite composites an attractive material for large scale water purification applications. Crystallinity as well as adsorption capacity was maintained somewhat under adsorption conditions. The optimal pH range was found to be near neutral-pH 7.

Chromate was adsorbed on the Fe_2O_3 as well. The surface area after functionalization decreases, but this did not appear to adversely affect the chromate adsorption, suggesting that adsorption occurs on the external surface. Adsorption is dependent on the loading of functional group and the surface charge, consistent with an electrostatic interaction. The adsorption capacity was .72 mmol/g for nanoscale and .845 mmol/g for commercial samples. These are attractive capacities and competitive with currently existing technologies. The maintenance of adsorption capacity coupled with the easy removal renders these magnetic zeolite composites an attractive material for large scale water purification applications.

Crystallinity as well as adsorption capacity was maintained under adsorption conditions. One potential drawback of this method is the low pH's required for optimal

adsorption capacity. Methods of adsorbing cations to the amine functional group to increase the optimal pH fro adsorption have been suggested for the future work. The pH is dependent on the solution states of the metal in question, and was shown to be different for chromate and arsenate in this work.

Future work could improve on the magnetism of these materials, attempt to address the iron leaching, or look at appropriate functional groups and conditions for adsorption of other contaminants. Improvements in the zeolite host such as increased external surface area would also be beneficial.

REFERENCES

1. Yokoi, T., T. Tatsumi, and H. Yoshitake, *Fe3+ coordinated to amino-functionalized MCM-41: an adsorbent for the toxic oxyanions with high capacity, resistibility to inhibiting anions, and reusability after a simple treatment.* Journal of Colloid and Interface Science, 2004. **274**(2): p. 451-457.

2. Habuda-Stanic, M., et al., *Quality of groundwater in eastern Croatia. The problem of arsenic pollution.* Desalination, 2007. **210**(1-3): p. 157-162.

3. Tosheva, L. and V.P. Valtchev, *Nanozeolites: Synthesis, Crystallization Mechanism, and Applications.* Chemistry of Materials, 2005. **17**(10): p. 2494-2513.

4. Song, W., et al., *Synthesis, Characterization, and Adsorption Properties of Nanocrystalline ZSM-5.* Langmuir, 2004. **20**(19): p. 8301-8306.

5. Rao, J., *A study on Environmental Characterization of Fly Ash and Its Response to Zeolite Syntheses.* Indian Journal of Environmental Protection, 2000. **20**(4): p. 290-296.

6. Murayama, N., et al., *Evaluation of Coal Fly Ash and Incineration Ash as Raw Material for Zeolite Synthesis.* Shigen-to-Sozai, 2001. **117**(6): p. 501-505.

7. Cl, T.B., C.D. Williams, and D. Apperley, *A study of the chemistry of isomorphous substitution and characterization of Al-ZSM-5 and Sc-ZSM-5 synthesized in fluoride media.* Inorganic Materials, 2007. **43**(7): p. 758-769.

8. Egeblad, K., et al., *Mesoporous zeolite and zeotype single crystals synthesized in fluoride media.* Microporous and Mesoporous Materials, 2007. **101**(1-2): p. 214-223.

9. Song, W., et al., *Size-Dependent Properties of Nanocrystalline Silicalite Synthesized with Systematically Varied Crystal Sizes.* Langmuir, 2004. **20**(11): p. 4696-4702.

10. Schoeman, B.J., Sterte, J. and Otterstedt, J.E., *Colloidal Zeolite Suspensions.* Zeolites, 1994. **14**: p. 110-115.

11. Li, Q., Creaser. Creaser, Derek, Sterte Johan, *An Investigation of the Nucleation/Crystallization Kinetics of nanosized Colloidal Faujasite Zeolites.* Chemistry of Materials, 2002. **14**: p. 1319-1324.

12. Richer, R., *Direct synthesis of functionalized mesoporous silica by non-ionic alkylpolyethyleneoxide surfactant assembly.* Chemm comm, 1998: p. 1775-1777.

13. Haggerty, G.M. and R.S. Bowman, *Sorption of chromate and other inorganic anions by organo-zeolite.* Environmental Science & Technology, 1994. **28**(3): p. 452-458.

14. White, M.A. and M. Lumsden, *Bonding of Organic Amino, Vinyl, and Acryl Groups to Nanometer-Sized NaX Zeolite Crystal Surfaces.* Langmuir, 2003. **19**(10): p. 4205-4210.

15. Margolese, D., et al., *Direct Syntheses of Ordered SBA-15 Mesoporous Silica Containing Sulfonic Acid Groups.* Chemistry of Materials, 2000. **12**(8): p. 2448-2459.

16. Oliveira, L.C.A., et al., *Magnetic zeolites: a new adsorbent for removal of metallic contaminants from water.* Water Research, 2004. **38**(17): p. 3699-3704.

17. Ellis, A.S., T.M. Johnson, and T.D. Bullen, *Chromium Isotopes and the Fate of Hexavalent Chromium in the Environment.* Science, 2002. **295**(5562): p. 2060-2062.

18. Faghihian, H. and R.S. Bowman, *Adsorption of chromate by clinoptilolite exchanged with various metal cations.* Water Research, 2005. **39**(6): p. 1099-1104.

19. Ghiaci, M., et al., *Adsorption of chromate by surfactant-modified zeolites and MCM-41 molecular sieve.* Separation and Purification Technology, 2004. **40**(3): p. 285-295.

20. Yoshitake, H., T. Yokoi, and T. Tatsumi, *Adsorption of Chromate and Arsenate by Amino-Functionalized MCM-41 and SBA-1.* Chemistry of Materials, 2002. **14**(11): p. 4603-4610.

21. *Case Studies in Environmental Medicine (CSEM)*. 2000, CDC.

22. *WHO | Arsenic in drinking water*. [cited; Available from: http://www.who.int/mediacentre/factsheets/fs210/en/

23. Dept of Health and Human Services Agency for Toxic, S., *Public Health Statement for Arsenic*. 2007.

24. *Arsenic: health effects, mechanisms of actions, and research issues*. 1999 [cited; Available from: http://www.ncbi.nlm.nih.gov/pmc/articles/PMC1566656/

25. Control, C.f.D. [cited.

26. Ackermann, J., et al., *Speciation of Arsenic under Dynamic Conditions.* Engineering in Life Sciences, 2008. **8**(6): p. 589-597.

27. Mintova, S., V. Valtchev, and G.P.l.-B.l. I. Kiricsi, *Synthesis of nanosized FAU-type zeolite*, in *Porous materials in environmentally friendly pocesses, Proceedings of the 1st international FEZA conference*. 1999, Elsevier. p. 141-148.

28. Song, W., et al., *Microscopic and Macroscopic Characterization of Organosilane-Functionalized Nanocrystalline NaZSM-5.* Langmuir, 2005. **21**(15): p. 7009-7014.

29. Bowman, R.S., *Applications of surfactant-modified zeolites to environmental remediation.* Microporous and Mesoporous Materials, 2003. **61**(1-3): p. 43-56.

30. Li, Z., Y. Zou, and R.S. Bowman, *Long-Term Chemical and Biological Stability of Surfactant-Modified Zeolite.* Environmental Science & Technology, 1998. **32**(17): p. 2628-2632.

31. Lim, M.H. and A. Stein, *Comparative Studies of Grafting and Direct Syntheses of Inorganic−Organic Hybrid Mesoporous Materials.* Chemistry of Materials, 1999. **11**(11): p. 3285-3295.

32. Rosenholm, J.M. and M. Linden, *Wet-Chemical Analysis of Surface Concentration of Accessible Groups on Different Amino-Functionalized Mesoporous SBA-15 Silicas.* Chemistry of Materials, 2007. **19**(20): p. 5023-5034.

33. Stein, A., B.J. Melde, and R.C. Schroden, *Hybrid Inorganic-Organic Mesoporous Silicates-Nanoscopic Reactors Coming of Age.* Advanced Materials, 2000. **12**(19): p. 1403-1419.

34. Li, J., et al., *Different N-containing functional groups modified mesoporous adsorbents for Cr(VI) sequestration: Synthesis, characterization and comparison.* Microporous and Mesoporous Materials, 2008. **110**(2-3): p. 442-450.

35. song, W., V.H. Grassian, and S.C. Larsen, *Hexagonal, hollow, aluminium-containing ZSM-5 tubes prepared from mesoporous silica templates.* Chem Comm, 2004.

36. Kuzniatsova, T., et al., *Zeta potential measurements of zeolite Y: Application in homogeneous deposition of particle coatings.* Microporous and Mesoporous Materials, 2007. **103**(1-3): p. 102-107.

37. Rimer, J.D., R.F. Lobo, and D.G. Vlachos, *Physical Basis for the Formation and Stability of Silica Nanoparticles in Basic Solutions of Monovalent Cations.* Langmuir, 2005. **21**(19): p. 8960-8971.

38. Turro, N.J., et al., *Photochemical and Magnetic Resonance Investigations of the Supramolecular Structure and Dynamics of Molecules and Reactive Radicals on the External and Internal Surface of MFI Zeolitess.* Journal of the American Chemical Society, 2000. **122**(47): p. 11649-11659.

39. LC Oliveira, D.I.P., Smaniotto, A., Pergher S. B.C., *Magnetic Zeolites: a new adsorbent for removal of metallic contaminants from water.* Water Research, 2004. **38**: p. 3699-3704.

40. Pergher, S.B.C., et al., *Materiais magnéticos baseados em diferentes zeólitas para remoção de metais em água.* Química Nova, 2005. **28**: p. 751-755.

41. Cao, J.L., et al., *Magnetic P zeolites: Synthesis, characterization and the behavior in potassium extraction from seawater.* Separation and Purification Technology, 2008. **63**(1): p. 92-100.

42. Chen, X., et al., *Synthesis of Highly Selective Magnetic Mesoporous Adsorbent.* The Journal of Physical Chemistry C, 2009. **0**(0).

43. Barquist, K. and S.C. Larsen, *Chromate adsorption on amine-functionalized nanocrystalline silicalite-1.* Microporous and Mesoporous Materials, 2008. **116**(1-3): p. 365-369.

44. Kuivila, C.S., J.B. Butt, and P.C. Stair, *Characterization of Surface Species on Iron Synthesis Catalysts by X-Ray Photoelectron-Spectroscopy.* App. Surf. Sci., 1988. **32**(1-2): p. 99-121.

45. Weckhuysen, B.M., et al., *Conversion of Methane to Benzene over Transition Metal Ion ZSM-5 Zeolites: II. Catalyst Characterization by X-Ray Photoelectron Spectroscopy.* Journal of Catalysis, 1998. **175**(2): p. 347-351.

46. Dong, J., Z. Xu, and S.M. Kuznicki, *Magnetic Multi-Functional Nano Composites for Environmental Applications.* Advanced Functional Materials, 2009. **19**(8): p. 1268-1275.

47. Kanthasamy, R., K. Barquist, and S.C. Larsen, *Transition metal and organic functionalization of hollow zeolite structures.* Microporous and Mesoporous Materials, 2008. **113**(1-3): p. 554-561.

48. Larsen, S.C., *Nanocrystalline Zeolites and Zeolite Structures: Synthesis, Characterization, and Applications.* The Journal of Physical Chemistry C, 2007. **111**(50): p. 18464-18474.

49. Cheng, C.-H., et al., *Functionalization of the Internal Surface of Pure-Silica MFI Zeolite with Aliphatic Alcohols.* The Journal of Physical Chemistry C, 2008. **112**(10): p. 3543-3551.

50. Zhan, B.-Z., M.A. White, and M. Lumsden, *Bonding of Organic Amino, Vinyl, and Acryl Groups to Nanometer-Sized NaX Zeolite Crystal Surfaces.* Langmuir, 2003. **19**(10): p. 4205-4210.

51. H.J. Ku, B.J.A., B.E. Jeon, and W. Chang,, Journal of Industrial and Engineering chemistry, 2005. **11**(6): p. 841

52. Dong, A., et al., *Fabrication of hollow zeolite microcapsules with tailored shapes and functionalized interiors.* Microporous and Mesoporous Materials, 2003. **64**(1-3): p. 69-81.

53. Li, Z., et al., *Enhanced Reduction of Chromate and PCE by Pelletized Surfactant-Modified Zeolite/Zerovalent Iron.* Environmental Science & Technology, 1999. **33**(23): p. 4326-4330.

54. Wang, J., et al., *Mesoporous MSU materials functionalized with sulfonic group: A multinuclear NMR and theoretical calculation study.* Microporous and Mesoporous Materials, 2006. **89**(1-3): p. 219-226.

55. Lam, K.F., K.L. Yeung, and G. McKay, *Selective mesoporous adsorbents for and Cu2+ separation.* Microporous and Mesoporous Materials, 2007. **100**(1-3): p. 191-201.

56. Salmio, H. and D. Bruhwiler, *Distribution of Amino Groups on a Mesoporous Silica Surface after Submonolayer Deposition of Aminopropylsilanes from an Anhydrous Liquid Phase.* The Journal of Physical Chemistry C, 2007. **111**(2): p. 923-929.

57. Shan, W., et al., *Magnetically Separable Nanozeolites: Promising Candidates for Bio-Applications.* Chemistry of Materials, 2006. **18**(14): p. 3169-3172.

58. Arruebo, M., et al., *Sustained release of doxorubicin from zeolite–magnetite nanocomposites prepared by mechanical activation.* Nanotechnology, 2006. **17**(16): p. 4057-4064.

59. Suh, W.H., Y.-H. Suh, and G.D. Stucky, *Multifunctional nanosystems at the interface of physical and life sciences.* Nano Today, 2009. **4**(1): p. 27-36.

60. Andersson, S.L.T. and R.F. Howe, *An x-ray photoelectron study of metal clusters in zeolites.* The Journal of Physical Chemistry, 1989. **93**(12): p. 4913-4920.

61. Burkett, S.L., S.D. Sims, and S. Mann, *Synthesis of hybrid inorganic–organic mesoporous silica by co-condensation of siloxane and organosiloxane precursors.* chemm Comm, 1996: p. 1367-1368.

62. L. Dambies, C.G., S. Yiacoumi, E. Guibal, Colloid Surf. A: Physicochem. Eng. Aspects 2001. **177**: p. 203.

63. Bailey, S.E.O., Trudy J.; Bricka,R. Mark; Adrian, D. Dean; , *A review of potentially low-cost sorbents for heavy metals.* Water Research, 1999. **33**.

64. Song, W., et al., *Development of Improved Materials for Environmental Applications: Nanocrystalline NaY Zeolites.* Environmental Science & Technology, 2005. **39**(5): p. 1214-1220.

65. Brito, F., et al., *Equilibria of chromate(VI) species in acid medium and ab initio studies of these species.* Polyhedron, 1997. **16**(21): p. 3835-3846.

66. Chuan, M.C. and J.C. Liu, *Release behavior of chromium from tannery sludge.* Water Research, 1996. **30**(4): p. 932-938.

67. Elizalde-González, M.P., J. Mattusch, and R. Wennrich, *Arsenic Speciation Analysis in Solutions Treated with Zeolites.* Microchimica Acta, 2005. **151**(3): p. 257-262.

68. Elizalde-González, M.P., et al., *Sorption on natural solids for arsenic removal.* Chemical Engineering Journal, 2001. **81**(1-3): p. 187-195.

69. Guan, X.-H., T. Su, and J. Wang, *Quantifying effects of pH and surface loading on arsenic adsorption on NanoActive alumina using a speciation-based model.* Journal of Hazardous Materials, 2009. **166**(1): p. 39-45.

70. Xu, Y.-h., T. Nakajima, and A. Ohki, *Adsorption and removal of arsenic(V) from drinking water by aluminum-loaded Shirasu-zeolite.* Journal of Hazardous Materials, 2002. **92**(3): p. 275-287.

71. Chutia, P., et al., *Arsenic adsorption from aqueous solution on synthetic zeolites.* Journal of Hazardous Materials, 2009. **162**(1): p. 440-447.

72. Zhang, H. and R.J. Bartlett, *Light-Induced Oxidation of Aqueous Chromium(III) in the Presence of Iron(III) - Environmental Science & Technology (ACS Publications).* Environmental Science and Technology, 1999. **33**(4): p. 588-594.

73. Kumar, P., et al., *Surface-modified Zeolite-A for sequestration of arsenic and chromium anions.* Current Science, 2007. **92**(4): p. 512-518.

74. Mayo, J.T.Y., S.; Yean, S.; Cong, L; Shipley, H.; Yu, W; Faulkner, J.; Kan, A.; Tomson, M.; Colvin, V.L., *The effect of nanocrystalline magnetitesizeon arsenic removal.* Science and Technologyof Advanced Materials, 2007. **8**: p. 71-75.

75. Payne, K., B.;Abdel-Fattah, Tarek, M., *Adsorption of Arsenate and Arsenite by Iron-Treated Activated Carbon and Zeolites: Effects of pH, Temperature, and Ionic Strength.* Journal of Environmental Science and Health. Part A, Toxic/hazardous Subsances and Evnironmental Engineering, 2005. **40**(4): p. 732-749.

76. Davila-Jiminez, M.M., et al., *In situ and ex situ study of the enhanced modification with iron of clinoptilolite-rich zeolitic tuff for arsenic sorption from aqueous solutions.* Journal of Colloid and Interface Science, 2008. **322**(2): p. 527-536.

77. Menhanje-Bena, R.K., H.; Shahaheri,S.; Ghazi-Khansari, M.; Hosseni, M., *Evaluation of iron modified zeolites for removal of arsenic from drinking water.* Studies in Surface Science and Catalysis, 2004. **154**: p. 1892-1899.

78. Song, W.G., et al., *Development of improved materials for environmental applications: Nanocrystalline NaY zeolites.* Environmental Science & Technology, 2005. **39**(5): p. 1214-1220.

79. Daus, B., H. Weiß, and R. Wennrich, *Arsenic speciation in iron hydroxide precipitates.* Talanta, 1998. **46**(5): p. 867-873.

80. /www.princeton.edu/~chm333/2003/arsenic/sources/chemistry.htm, *An Eh-pH diagram of aqueous, aerobic As-solution at 25 C and 1 bar of pressure. (Smedley)*. 2003.

81. Smedley, P.L., and D.G. Kinniburgh. Applied Geochemistry, *A review of the source, behavior and distribution of arsenic in natural waters.* Applied Geochemistry, 2002. **17**: p. 517-586.